Grey-Box Modeling and Validation of Deoiling Hydrocyclones

Bram, Mads Valentin

Publication date:
2020

Document Version
Publisher's PDF, also known as Version of record

GREY-BOX MODELING AND VALIDATION OF DEOILING HYDROCYCLONES

BY
MADS VALENTIN BRAM

DISSERTATION SUBMITTED 2020

AALBORG UNIVERSITY
DENMARK

Grey-Box Modeling and Validation of Deoiling Hydrocyclones

Ph.D. Dissertation

Mads Valentin Bram

Dissertation submitted September 23, 2020

Dissertation submitted: September 23, 2020

PhD supervisor: Associate Prof. Zhenyu Yang
Aalborg University

PhD committee: Associate Professor Ben-Guang Rong (chairman)
Aalborg University

Professor John Bagterp Jørgensen
Technical University of Denmark

Associate Professor Christian Holden
Norwegian University of Science and Technology

PhD Series: Faculty of Engineering and Science, Aalborg University

Department: Department of Energy Technology

ISSN (online): 2446-1636
ISBN (online): 978-87-7210-814-8

Published by:
Aalborg University Press
Kroghstræde 3
DK – 9220 Aalborg Ø
Phone: +45 99407140
aauf@forlag.aau.dk
forlag.aau.dk

Printed in Denmark by Rosendahls, 2020

Abstract

The produced oil and gas from offshore installations are transported to onshore facilities for further processing, while the produced water (PW), which commonly is more than 90% of the produced mixture by volume, has to be cleaned before it is discharged to the surrounding sea. Danish regulations require the discharged oil-in-water (OiW) concentration to be less than 30ppm on a weekly average, and less than 222t total oil discharge annually. However, these restrictions are very likely to become stricter due to governmental trends toward zero harmful discharge.

Current control solutions for produced water treatment (PWT) suffer from a set of problems associated with the produced water treatment processes being interdependent, and sometimes contradictory. The challenges call for solutions based on plant-wide control, which benefits from accurate and reliable control-oriented models of the processes, such as models of the deoiling hydrocyclones. The field of research of computational fluid dynamics and data-driven black-box hydrocyclone models are relatively mature and provide a good background for understanding the separation principles of a hydrocyclone. However, the model must be relatively simple for control design purposes. Additionally, the model will likely perform better in a broader range of operating conditions if it is derived from first principles.

A grey-box model structure is proposed that uses hydrocyclone valves and existing measurements as input to predict various separation performance metrics, such as grade efficiency, also called mitigation probability, and separation efficiency. The model structure is composed of valve dynamics from electrical input to actual valve opening, virtual flow resistance (VFR) to estimate flow rates and pressures, and oil droplet trajectory (ODT) to classify oil droplets. Each main part of the model was experimentally validated on a modified PWT pilot plant, including OiW measurements obtained from real-time fluorescence-based monitors, and showed good accuracy and reliability.

In this thesis, a versatile control-oriented grey-box model structure of a deoiling hydrocyclone with emphasis on practical implementation is defined, analyzed, and validated. An approach to obtain or identify all parameters of

the model is proposed and validated. A proposed pin-cart model was formulated and identified to describe the dynamics of the valves located at the hydrocyclone outlets. The pin-cart model was validated using actual valve data, and was able to reasonably describe the longer perceived delay when changing valve direction. A VFR model was proposed and identified using measurements obtained from the PWT pilot plant. The VFR model was able to predict the flow rates and pressures of the hydrocyclone with good accuracy. The ODT model was validated using real-time fluorescence-based OiW monitors, while addressing the challenges associated with using the OiW monitors for validation. However, it is acknowledged that the proposed model structure can always benefit from further validation, such as by droplet size measurements. Additionally, the modular model structure allows future works to incorporate effects, such as droplet coalescence and breakup. The model is deemed valuable for control design and other observer-related purposes.

Resumé

Det producerede olie og gas fra offshore-installationer transporteres til onshore-faciliteter til yderligere forarbejdning, mens det producerede vand, der almindeligvis udgør mere end 90% af den producerede blanding, skal renses, før det udledes til det omkringliggende hav. Danske lovgivninger kræver, at det ugentlige gennemsnit af udledt oliekoncentration er mindre end 30ppm og at der udledes mindre end 222t olie årligt. Dog vil disse begrænsninger meget sandsynligt blive strengere på grund af politiske planer for ingen udledning af skadelige stoffer.

Nuværende kontrolløsninger til olieudskilleranlæg lider af et sæt problemer forbundet med at behandlingsprocesserne er indbyrdes afhængige og nogle gange modstridende. Udfordringerne kræver løsninger baseret på anlægsomfattende proceskontrol, som drager fordel af nøjagtige og pålidelige modeller af processerne, såsom modeller af olieudskiller hydrocykloner. Forskningsområdet for CFD og datadrevne hydrocyklonmodeller er relativt velkendt og giver en god baggrund for forståelse af hydrocyklonernes separationsprincipper. Modellen skal dog være relativt enkel for at kunne anvendes til kontroldesign. Derudover vil modellen sandsynligvis estimere bedre i et bredere omfang af driftsforhold, hvis modellen er udledt af første principper.

En grey-box-modelstruktur er foreslået, som bruger hydrocyklonens ventiler og de eksisterende målinger som input for at estimere ydeevne, såsom separationseffektivitet og effektivitet som funktion af oliedråbestørrelse. Modelstrukturen er sammensat af ventildynamik fra det elektriske input til den faktiske ventilåbning, virtuel modstand til at estimere strømningshastighed og tryk, og oliedråbernes banekurver til at klassificere oliedråberne. Hver hoveddel af modellen blev eksperimentelt valideret på et modificeret olieudskilleranlæg, hvor oliekoncentration blev målt af fluorescensbaserede sensorer som er blevet eftervist til at have god nøjagtighed og pålidelighed. I denne afhandling defineres, analyseres og valideres en alsidig kontrolorienteret grey-box-modelstruktur af en olieudskiller hydrocyklon med henblik på praktisk implementering. En fremgangsmåde til at opnå eller identificere alle parametre i modellen er foreslået og valideret. En pin-cart model blev formuleret og identificeret til at beskrive dynamikken i ventilerne, som er pla-

ceret ved hydrocyklonens udløb. Pin-cart modellen blev valideret ved hjælp af ventildata og var i stand til at beskrive den forsinkelse når ventilen ændrer retning. Modellen, baseret på virtuel modstand, blev identificeret ved hjælp af målinger opnået fra et olieudskilleranlæg og var i stand til at forudsige hydrocyklonens strømningshastigheder og tryk med god nøjagtighed. Modellen, baseret på oliedråbernes banekurver, blev valideret ved hjælp af fluorescensbaseret sensorer, samtidig med at adressere udfordringerne forbundet med at bruge realtidsmålinger af oliekoncentration til validering. Der erkendes at den foreslåede modelstruktur kan drage fordel af yderligere validering, f.eks. med målinger af oliedråbestørrelser. Derudover tillader den modulære modelstruktur at effekter kan inkorporeres, såsom dråbeforening og opbrud. Modellen anses for at være værdifuld for kontroldesign og andre observatørrelaterede formål.

Contents

Thesis Details

Thesis Title:	Grey-box modeling and validation of deoiling hydrocyclones
Ph.D. Student:	Mads Valentin Bram
Supervisor:	Associate Prof. Zhenyu Yang, Aalborg University

The body of the thesis consists of the following papers:

[A] M. V. Bram, L. Hansen, D. S. Hansen, and Z. Yang, "Grey-Box modeling of an offshore deoiling hydrocyclone system", in *2017 IEEE Conference on Control Technology and Applications (CCTA)*. Mauna Lani, HI, USA: IEEE, 27-30 August 2017, pp. 94-98. doi: 10.1109/CCTA.2017.8062446

[B] M. V. Bram, L. Hansen, D. S. Hansen, and Z. Yang, "Hydrocyclone Separation Efficiency Modeled by Flow Resistances and Droplet Trajectories", *IFAC-PapersOnLine* vol. 51, no. 8, pp. 132-137, 2018. doi: 10.1016/j.ifacol.2018.06.367

[C] M. V. Bram, L. Hansen, D. S. Hansen, and Z. Yang, "Extended Grey-Box Modeling of Real-Time Hydrocyclone Separation Efficiency", in *2019 18th European Control Conference (ECC)*. Naples, Italy: IEEE, 25-28 June 2019. pp. 3625-3631. doi: 10.23919/ECC.2019.8796175

[D] M. V. Bram, J. P. Calliess, S. Roberts, D. S. Hansen, and Z. Yang, "Analysis and Modeling of State-Dependent Delay in Control Valve", *IFAC-PapersOnLine*, 2020. [Accepted/In press]

[E] M. V. Bram, S. Jespersen, D. S. Hansen, and Z. Yang, "Control-Oriented Modeling and Experimental Validation of a Deoiling Hydrocyclone System", *Processes*, vol. 8, no. 9, pp. 1-33, 2020. doi: 10.3390/pr8091010

In addition the following publications have also been made:

[1] D. S. Hansen, M. V. Bram, and Z. Yang, "Efficiency investigation of an offshore deoiling hydrocyclone using real-time fluorescence- and microscopy-based monitors", in *2017 IEEE Conference on Control Technology and Applications (CCTA)*. Mauna Lani, HI, USA: IEEE, 27-30 August 2017, pp. 1104–1109. doi: 10.1109/CCTA.2017.8062606

[2] D. S. Hansen, M. V. Bram, P. Durdevic, S. Jespersen, and Z. Yang, "Efficiency evaluation of offshore deoiling applications utilizing real-time oil-in-water monitors", in *Proceedings of OCEANS'17 MTS/ IEEE Anchorage*, Anchorage, AK, USA: IEEE, 18 - 21 September 2017, pp. 1-6

[3] D. S. Hansen, S. Jespersen, M. V. Bram, and Z. Yang, "Uncertainty Analysis of Fluorescence-Based Oil-in-Water Monitors for Oil & Gas Produced Water", *Sensors*, vol. 20, no. 16, pp. 1-36, 2020. doi: 10.3390/s20164435

[4] D. S. Hansen, S. Jespersen, M. V. Bram, and Z. Yang, "Human Machine Interface Prototyping and Application for Advanced Control of Offshore Topside Separation Processes", in *IECON 2018 - 44th Annual Conference of the IEEE Industrial Electronics Society*, Washington, DC, USA: IEEE, 21 - 23 October 2018, pp. 2341–2347. doi: 10.1109/IECON.2018.8591309

[5] E. K. Nielsen, M. V. Bram, J. Frutiger, G. Sin, and M. Lind, "Modelling and Validating a Deoiling Hydrocylone for Fault Diagnosis using Multilevel Flow Modeling", in *International Symposium on Future I&C for Nuclear Power Plants*, Gyeongju, Korea, 24 - 30 November 2017, pp. 1–9

[6] E. K. Nielsen, M. V. Bram, J. Frutiger, G. Sin, and M. Lind, "A water treatment case study for quantifying model performance with multilevel flow modeling", *Nuclear Engineering and Technology*, vol. 50, no. 4, pp. 532–541, 2018. doi: 10.1016/j.net.2018.02.006

[7] M. V. Bram, A. Hassan, D. S. Hansen, P. Durdevic, S. Pedersen, and Z. Yang, "Experimental modeling of a deoiling hydrocyclone system", in *2015 20th International Conference on Methods and Models in Automation and Robotics (MMAR)*, Miedzyzdroje, Poland: IEEE, 24 - 27 August 2015, pp. 1080-1085. doi: 10.1109/MMAR.2015.7284029

[8] P. Durdevic, C. S. Raju, M. V. Bram, D. S. Hansen, and Z. Yang, "Dynamic oil-in-water concentration acquisition on a pilot-scaled offshore water-oil separation facility", *Sensors*, vol. 17, no. 1, pp. 1-11, 2017. doi: 10.3390/s17010124

Other publications which are not directly relevant for this Ph.D. thesis:

[9] K. L. Jepsen, M. V. Bram, S. Pedersen, and, Z. Yang, "Membrane Fouling for Produced Water Treatment: A Review Study From a Process Control Perspective", *Water*, vol. 10, no. 7, pp. 1-28, 2018. doi: 10.3390/w10070847

[10] K. L. Jepsen, M. V. Bram, L. Hansen, S. M. Ø. Lauridsen, and, Z. Yang, "Online Backwash Optimization of Membrane Filtration for Produced Water Treatment", *Membranes*, vol. 7, no. 6, pp. 1-18, 2017. doi: 10.3390/membranes9060068

Preface

This thesis is submitted as a collection of papers to fulfill the requirements for the degree of Doctor of Philosophy at the Department of Energy Technology, Aalborg University, Denmark. The work was carried out at the Department of Energy Technology, Aalborg University Campus Esbjerg, from September 2017 to September 2020 under the supervision of Associate Professor Zhenyu Yang. During the project period I was a visiting researcher in the Machine Learning Reasearch Group, Department of Engineering, Oxford University, United Kingdom, from April 2019 to June 2019 under the supervision of Associate Professor Jan-Peter Calliess and Professor Stephen Roberts. The project has been supported by Danish Hydrocarbon Research and Technology Centre and Aalborg University joint project (Grey-Box Modeling and Plant-wide Control, Aalborg University, Pr-no: 878041).

I gracefully thank all colleagues from the Department of Energy Technology, Aalborg University for providing a bright and encouraging research environment. I would like to thank my supervisor Zhenyu Yang for his unrelenting positive support as supervisor and friend. I would also like to thank Associate Professor Jan-Peter Calliess, Professor Stephen Roberts, and their talented research team for providing an excellent and inspiring stay at Oxford University. I gratefully thank my project colleagues Leif Hansen, Stefan Jespersen, Kasper L. Jepsen, Simon Pedersen, and Petar Durdevic for many valuable discussions and collaborations. Special thanks to my colleague, and former fellow student, Dennis S. Hansen for more than nine years of professional teamwork and personal developments.

In addition I would like to thank my family for their support and encouragement. Finally, I would like to express my sincere gratitude towards my friends, and especially my girlfriend for supporting me through tough and stressful times.

Mads Valentin Bram
Aalborg University

Abbreviations

ANN	Artificial neural networks
ARMAX	Autoregressive–moving-average model with exogenous inputs
BIBO	Bounded-input bounded-output
CFD	Computational fluid dynamics
FDD	Fault detection and diagnosis
FOPDT	First-order-plus-dead-time
MAE	Mean average error
MAE_f	Filtered mean average error
MPC	Model predictive control
NPV	Net present value
ODT	Oil droplet trajectory
OiW	Oil-in-water
PID	Proportional, integral, and derivative
PW	Produced water
PWT	Produced water treatment
RFU	Relative fluorescence units
RNN	Recurrent neural network
SISO	Single-input single-output
SSE	Sum of squared error
SSE_r	Relative sum of squared error
VFR	Virtual flow resistance

Nomenclature

$[r, z]$	Radial and axial coordinates (m)
$[v_r, v_z]$	Dispersed phase radial and axial speed (m/s)
$[W, U_c, T]$	Continuous phase axial, radial, and tangential velocity fields (m/s)
α	Hydrocyclone inlet speed imperfection coefficient $(-)$
$\beta_{1,2}$	Hydrocyclone cone angles $(^\circ)$
$\boldsymbol{\theta}$	Set of all coefficients for $Y(\hat{r})$ $(-)$
$\boldsymbol{K}$	Set of all virtual hydrocyclone flow conductance constants $(\frac{\mathrm{L}^2}{\mathrm{bar}\cdot\mathrm{s}^2})$
$\boldsymbol{u_{ext}}$	Vector of uncontrollable inputs $(-)$
$\boldsymbol{u_{ref}}$	Vector of valve input references (%)
$\boldsymbol{u_V}$	Vector of actual valve openings (%)
$\boldsymbol{y_{met}}$	Vector of hydrocyclone performance metrics $(-)$
$\Delta\rho$	Density difference between dispersed and continuous phase $(\mathrm{kg/m^3})$
ΔP_{io}	Pressure difference between hydrocyclone inlet and overflow (bar)
ΔP_{iu}	Pressure difference between hydrocyclone inlet and underflow (bar)
Δy_{max}	Maximum valve speed (%)
Δy_{min}	Minimum valve speed (%)
μ	Continuous phase dynamic viscosity $(\mathrm{Pa}\cdot\mathrm{s})$
ϕ_i	Volumetric hydrocyclone inlet droplet size distribution $(-)$
ϕ_u	Volumetric hydrocyclone underflow droplet size distribution $(-)$
$\theta_{1,2,3,4}$	Coefficients for $Y(\hat{r})$ $(-)$
ε_{oil}	Volumetric oil removal from inlet to underflow (%)
ε_{red}	Concentration reduction from inlet to underflow (%)
A_L	Area of the envelope of zero axial velocity $(\mathrm{m^2})$
a_p, b_p, c_p	Coefficients for position-dependent pin speed $(-)$
B_L	Cart width (%)
C_i	Volumetric hydrocyclone inlet oil-in-water concentration (ppm)

C_u	Volumetric hydrocyclone underflow oil-in-water concentration (ppm)
D_d	Oil droplet diameter (m)
$D_{d_{100}}$	Smallest droplet diameter with 100% chance of being separated (m)
$D_{d_{50}}$	Droplet diameter with 50% chance of being separated (m)
$D_{o,i,n,u}$	Hydrocyclone segment diameters (m)
e	Valve position error (%)
e_{VFR}	Error of the virtual flow resistance model $(-)$
F_s	Volumetric flow split (%)
f_{V_o}	Function between overflow valve reference and actual opening $(-)$
f_{V_u}	Function between underflow valve reference and actual opening $(-)$
G	Grade efficiency (%)
H_{liquid}	Separator tank liquid level (m)
H_{oil}	Separator tank oil level (m)
H_{water}	Separator tank water level (m)
$K_{i,u,o}$	Virtual hydrocyclone flow conductance constants $(\frac{\mathrm{L}^2}{\mathrm{bar}\cdot\mathrm{s}^2})$
K_{V_u,V_o1,V_o2}	Underflow and overflow valve flow conductance constants $(\frac{\mathrm{L}^2}{\mathrm{bar}\cdot\mathrm{s}^2})$
$L_{1,2,3,4}$	Hydrocyclone segment axial lengths (m)
N	Total number of discrete droplet diameters $(-)$
n	Forced/free vortex coefficient $(-)$
N_p	Total number of free valve model parameters $(-)$
N_{100}	Index to the smallest discrete droplet diameter with 100% chance of being separated $(-)$
N_{dp}	Total number of data points $(-)$
O_V	Output of the internal valve control $(-)$
$OiW_{i1,i2}$	Inlet oil-in-water calibration data (ppm)
$OiW_{u1,u2}$	Underflow oil-in-water calibration data (ppm)
P_k	Proportional gain $(-)$
P_{is}	Absolute hydrocyclone inlet sidestream pressure (bar)
P_i	Absolute hydrocyclone inlet pressure (bar)
P_j	Absolute virtual hydrocyclone junction pressure (bar)
P_{ob}	Absolute hydrocyclone overflow back pressure (bar)
P_o	Absolute hydrocyclone overflow pressure (bar)
P_{sep}	Absolute separator tank pressure (bar)

P_{ub}	Absolute hydrocyclone underflow back pressure (bar)
P_u	Absolute hydrocyclone underflow pressure (bar)
PDR	Pressure drop ratio $(-)$
Q_i	Volumetric hydrocyclone inlet flow rate (L/s)
Q_o	Volumetric hydrocyclone overflow flow rate (L/s)
Q_r	Volumetric flow rate across envelope of zero axial velocity (L/s)
Q_u	Volumetric hydrocyclone underflow flow rate (L/s)
Q_{for}	Volumetric flow rate moving towards the underflow at Z_2 (L/s)
Q_{in}	Volumetric separator tank inlet flow rate (L/s)
Q_{is}	Volumetric hydrocyclone inlet sidestream flow rate (L/s)
Q_{rev}	Volumetric flow rate moving towards the overflow at Z_2 (L/s)
Q_{us}	Volumetric hydrocyclone underflow sidestream flow rate (L/s)
R^2	Coefficient of determination (%)
R_d	Radial starting position of critical oil droplet trajectory (m)
R_L	Radius of locus of zero axial velocity (m)
R_R	Recirculation rate $(-)$
R_z	Hydrocyclone inner wall radius (m)
$R_{i,u,o}$	Virtual hydrocyclone orifices $(-)$
Re	Reynolds number $(-)$
$S_{1,2,3,4}$	Hydrocyclone segments $(-)$
U_d	Settling speed (m/s)
U_L	Radial speed from draining across envelope of zero axial velocity (m/s)
u_{V_o}	Overflow valve input reference (%)
u_{V_u}	Underflow valve input reference (%)
v_i	Hydrocyclone inlet speed (m/s)
V_D	Hydrocyclone inlet sidestream discard valve (%)
V_{gas}	Separator tank gas control valve (%)
V_{is}	Hydrocyclone inlet sidestream control valve (%)
V_i	Hydrocyclone inlet control valve (%)
V_{oil}	Separator tank oil control valve (%)
V_o	Hydrocyclone underflow control valve (%)
V_R	Hydrocyclone inlet sidestream return valve (%)
V_{top}	Separator tank top side control valve (%)
V_{ub}	Hydrocyclone underflow back pressure control valve (%)

V_{us}	Hydrocyclone underflow sidestream control valve (%)
V_u	Hydrocyclone underflow control valve (%)
W_s	Axial speed scale due to draining across envelope of zero axial velocity $(-)$
Y	Axial velocity profile (m/s)
y	Pin position (%)
$Z_{0,1,2,3,4}$	Axial coordinate of hydrocyclone segments (m)
$\bar{}$	Global mean value
$\check{}$	Integration variable
$\hat{}$	Normalized value

Part I

Extended Summary

Chapter 1

Introduction and Motivation

As the world's total primary energy supply transitions to renewable sources, the total energy demand is predicted to increase from 662 exajoules in 2019 to 961 exajoules in 2050, at which scale the total supply of oil and gas are still estimated to increase by 0.6% to satisfy the increased demand [1]. Offshore oil and gas production will face a difficult challenge of treating the steadily increasing amount of produced water (PW) during this transition. Over the lifetime of a producing hydrocarbon reservoir, several methods are deployed to increase yield, such as the injection of water, steam, gases, and other chemicals. Producers in the Danish sector of the North Sea started injecting water in 1985 to such an extent that the extracted mixture is more than 90% water by volume (water cut) [2–7]. In addition, the produced oil quantity from the reservoirs declines over time to such a degree that Denmark stopped being self-sufficient on oil in 2018 [8]. These issues change the question: "How much oil can be extracted?" into: "How long can the operation continue to be economically viable?" when the profits decline over time [9]. The Danish oil, gas, and water production over time are shown in Fig. 1.1.

To avoid the large economic piping and pumping costs of transporting the large quantity of PW to onshore facilities, the PW is treated offshore and discharged to the sea [4]. Even though the PW undertakes several stages of cleaning, small contents of dispersed and dissolved oil still remain, which introduces a set of environmental concerns [11–18]. Various national laws and regional regulations determine the legal discharge concentration and quantity thresholds that the industry must comply with. These regulations, generally become stricter and converges toward zero harmful discharge [7, 12, 18]. For the Danish part of the North Sea, the PW must be sampled at least twice every day and have an oil-in-water (OiW) concentration of less than 30ppm [19]. Additionally, the total annual quantity of oil discharged in the Danish sector of the North Sea must be less than 222t [20]. This oil discharge

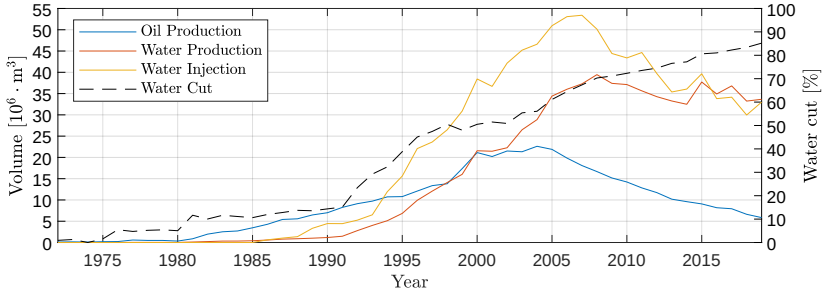

Fig. 1.1: Produced oil and water, and water injected from 1972 to 2019 in the Danish sector of the North Sea. Figure is generated using data from the Danish Energy Agency [10].

limit is specificity 202t for former Mærsk Oil in 2015 [20]. The increasing water cut and PW quantity render the limit of total discharged oil increasingly challenging to comply with, especially as the annual oil discharge from former Mærsk Oil was ∼193t in 2015 [20].

The remaining of this chapter is organized as follows: Section 1.1 describes the background and challenges for produced water treatment (PWT), Section 1.2 describes the motivation for improving the control-oriented models, Section 1.3 describes the problem and motivation for each included paper contribution.

1.1 Background

The common offshore PWT train includes separator tanks, and in more than 90% of cases, also deoiling hydrocyclones, as illustrated in Fig. 1.2 [21–28]. Separator tanks are used in the first stages of PWT to separate the gas, oil, and water by density difference [7, 29]. Within the tanks, gas fills the top, water fills in the bottom, and oil settles on the water surface, where it eventually skims over a baffle into the oil chamber. The size and shape of the separator tanks vary greatly depending on operation and purpose. Typically, the water outlet of the separator tanks has an OiW concentration of 200-1000ppm, which is directed to the deoiling hydrocyclones to further reduce the OiW concentration [24, 30].

1.1.1 Hydrocyclones

Hydrocyclones were introduced after World War II by the Dutch State Mines as a new tool to separate dispersed solids from liquid, where some of the earliest most significant research was done by [32] for separating solids from liquid [33]. Hydrocyclones were later adopted to the offshore industry for

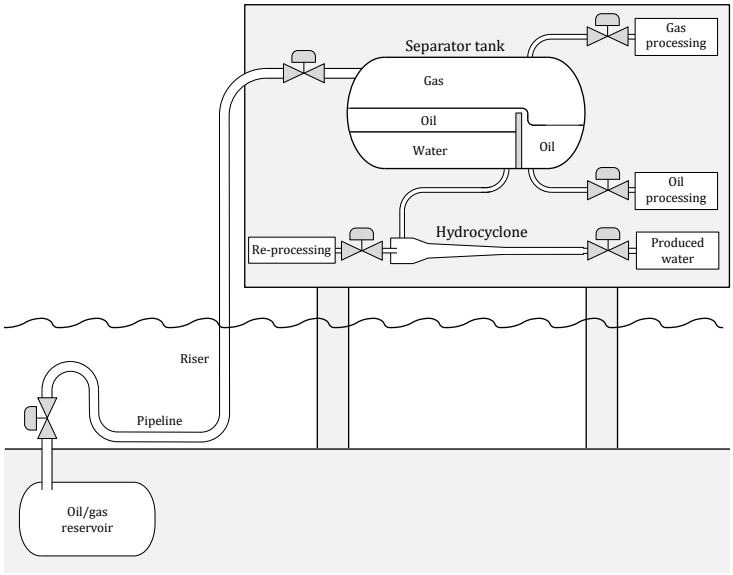

Fig. 1.2: Simplified overview of a current offshore produced water treatment train. Figure is based on illustrations from [31].

liquid-liquid separation in the 1980s, and currently deployed in many industrial applications [34–36].

Hydrocyclones have the benefit of no moving parts, low space and weight footprint, fast start-up, no additional pumping required, and ability to handle large quantities of flow compared to membrane filtration and flotation units, [7, 24, 27, 34, 37, 38]. Offshore deoiling hydrocyclones further reduce the OiW concentration of the PW down to $17-45$ppm such that the water may be re-used or discharged [7, 19, 24, 37]. Hydrocyclones utilize rotating flow to expose the fluid to high accelerations in order to enhance the separation by density difference [7, 37, 38]. Dense materials will be forced towards the wall of the cyclone (in this case water), and lighter materials will migrate towards the center of the rotating flow (in this case oil) [7, 37–39]. The PW leaves through the underflow, and the rejected oily water leaves through the overflow, as illustrated in Fig. 1.3.

1.1.2 Control Strategy

A simplified version of the three-phase separator and the deoiling hydrocyclone system is shown in Fig. 1.4. The oil-water interphase level (H_{water}) is typically maintained at a reference level, by a controller actuating the underflow valve (V_u) using H_{water} as feedback, to avoid the free oil to reach the

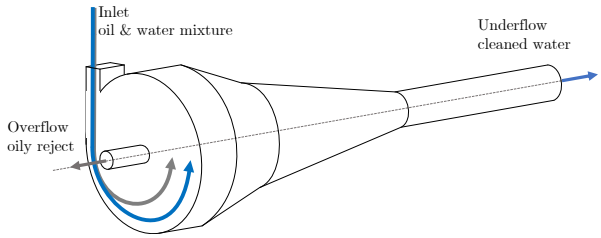

Fig. 1.3: Hydrocyclone operating principle. Figure is modified from Paper E.

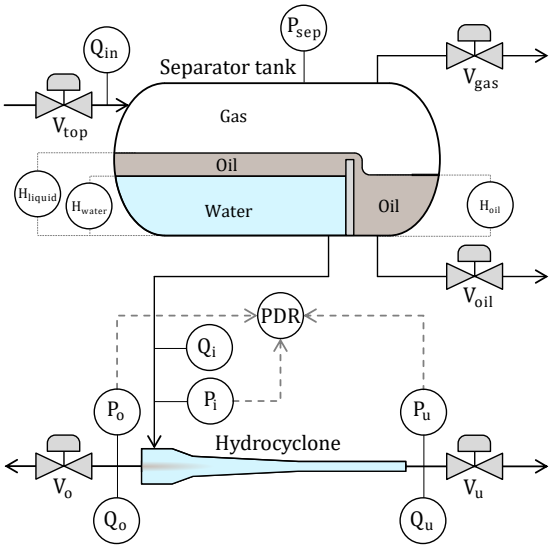

Fig. 1.4: Simplified PWT system overview. Figure is based on illustrations from [40].

water outlet, and avoid water spilling over the baffle, as illustrated in Fig. 1.4 [7, 29, 41]. The actuation of V_u and the effects thereof significantly affect hydrocyclone separation performance. To reduce these effects, a fixed hydrocyclone flow split defined as

$$F_s = \frac{Q_o}{Q_i} \approx \frac{Q_o}{Q_u} \,, \tag{1.1}$$

is typically maintained by a controller, where Q_i, Q_u, and Q_o are the volumetric inlet, underflow, and overflow flow rate, respectively. This controller actuates the overflow valve (V_o) using the pressure drop ratio defined as

$$PDR = \frac{\Delta P_{io}}{\Delta P_{iu}} = \frac{P_i - P_o}{P_i - P_u} \,, \tag{1.2}$$

as feedback, where P_i, P_u, and P_o are the inlet, underflow and overflow pressure, respectively [26, 42]. PDR is a reasonable intermediate variable as F_s has been proven to be monotonically increasing with PDR [26, 42]. The target steady-state PDR is typically $1.5-3$ for industrial applications and selected based on experience or empirical studies [34, 43, 44]. The choice of using PDR as feedback is primarily due to the accessibility, reliability, and accuracy of pressure transmitters. However, PDR is not a direct measure of hydrocyclone separation performance, but rather an intermediate variable. When evaluating hydrocyclone separation performance, two metrics are commonly used: concentration reducing separation efficiency defined as

$$\varepsilon_{red} = 1 - \frac{C_u}{C_i} \,, \tag{1.3}$$

and the volumetric oil removal separation efficiency defined as

$$\varepsilon_{oil} = \frac{C_o Q_o}{C_i Q_i} = 1 - \frac{C_u Q_u}{C_i Q_i} \,, \tag{1.4}$$

where C_i and C_u are the inlet and underflow volumetric OiW concentration, respectively. Equation (1.3) describes the percentage reduction of OiW concentration from inlet to underflow [37, 45]. Equation (1.4) describes the percentage of volumetric oil removal [46, 47]. As there are several issues with measuring reliable OiW concentrations in real-time, PDR is favored as the control objective.

A commonly deployed control strategy of the offshore separation system includes a list of proportional, integral, and derivative (PID) controllers as summarized in Table 1.1 [29, 34, 42, 43].

Table 1.1: Example of the control solutions deployed for offshore deoiling.

Control	Actuator	Feedback
Flow split	V_o	PDR
Oil-water interphase	V_u	H_{water}
Oil level	V_{oil}	H_{oil}
Separator tank pressure	V_{gas}	P_{sep}

The issues and challenges associated with this control strategy are well reviewed in [48], and can be summarized as:

- Hydrocyclone separation performance is significantly dependent on Q_i, which is determined from the oil-water interphase controller that actuates V_u [49, 50].
- A too aggressive oil-water interphase controller will propagate the variations of separator tank inlet flow rate (Q_{in}) downstream. Additionally,

this can cause V_u to become saturated at fully closed resulting in poor hydrocyclone performance [26, 40, 41, 49–53].

- PDR is significantly dependent on V_u, which can counteract and saturate the actuation of the flow split controller [30, 40, 49].
- The oil-water interphase controller is designed to keep H_{water} at a reference. However, this is not crucial as long as H_{water} is within a safety range [40].
- The relationship between PDR and ε_{oil} is uncorrelated in some operating conditions, and is an ongoing investigation topic [49, 54–56].

Common for these challenges is the fact that the systems are interconnected, such that the effect of actuating a single valve of one system, affects several other systems in various degrees of magnitude [50, 56]. The controllers being designed individually and often in a trial-and-error approach, often lack the knowledge of how it implicates the combined system performances [53, 57]. Experimental studies have investigated a solution for these challenges by deploying advanced control methods, such as model predictive control (MPC) and H_∞, with promising results [40, 52, 56, 58].

1.2 Motivation

A substantial amount of studies have investigated the internal hydrocyclone flows, pressures, performance metrics, and the effect of geometries by computational fluid dynamics (CFD) modeling [59–62]. A significant amount of the developed CFD models have been proven valid by experimental validation, such as in [60, 63]. While CFD models can be accurate, the computational intensity renders these models not suitable for control design. On the contrary, there exist several data-driven model approaches to model the hydrocyclone system that only concerns the input-output relationships without attempting to describe and without knowledge of the internal fluid dynamics. While these black-box methods such as autoregressive–moving-average model with exogenous inputs (ARMAX) models or artificial neural networks (ANN), as in [64, 65], can be accurate and tailor-made for control design, they require:

- Good quality and quantity of data.
- Reasonable choice of model structure.
- Reasonable balance between model complexity and computation time.

Failing to comply with these requirements will cause the obtained black-box model to perform poorly, especially in operating conditions that are not represented in the training data. Obtaining a sufficient quantity of data with persistent excitation is difficult, as the data are either rare or must be obtained by performing tests on the offshore facilities, which is expensive. An alternative is to pursuit a modelless solutions, such as the Extremum Seeking method [66]. Retrofit solutions, such as software updates to the existing control of the PWT, are favored as installation of new equipment and corresponding maintenance is expensive [27, 67]. As a result of these limitations, there is an incentive to combine the first principle modeling approaches and the data-driven approaches into one model framework. By combining these approaches, both the understood system knowledge and the available system data can contribute to the design of the model structures and parameter identifications.

1.2.1 Motivation for Grey-Box Modeling

Some of the earliest results of estimating the droplet diameter with 50% chance to be separated by the hydrocyclone ($D_{d_{50}}$) are done in [68]. Promising results have been made to describe the hydrocyclone fluid dynamics analytically, with a fixed F_s [69, 70]. However, the real system is likely to have variations in F_s during operation, which may cause the model to perform poorly [71]. Additionally, the flow rates are required to be known, well-calibrated, and reliable, which might not be available.

The lack of accumulation volume, and absence of compressible gas, renders the hydrocyclone system much faster than the three-phase separator tank system. The dynamic relationships between pressures drops and flow rates of the hydrocyclone can be considered so fast that modeling these dynamics introduces unwanted extra complexity and computation costs with insignificant improvements to the prediction performance. Due to the small volume, the residence time inside the hydrocyclone is typically $\sim 2s$ [7, 71].

There is an incentive to use separation-based grey-box hydrocyclone models for MPC solutions, such as in [58], to enable defining constraints, such as maximum OiW concentration of the discharged water. The defined model must have a relatively low computation cost to be used for MPC control [66].

Motivation for Dynamical Modeling of Control Valves

The slowest dynamics of the hydrocyclone are often from the associated control valves, and should be the main focus for describing the most dominant dynamical features of the system. Control valves are commonly deployed with pre-installed internal valve position controllers from the manufacturer, that aims to actuate the valve position to an externally provided reference.

However, as control valves are physical systems with moving parts, they exert undesired dynamical behaviors, such as hysteresis and deadband, that are reviewed and described in [72, 73]. As valves have vastly diverse characteristics, there is an incentive to define the hydrocyclone model structure to include the valves as an interchangeable model block, such that the valve model can be tailor-made to the specific application.

Motivation for Modeling Separation Performance

While the dynamic fluid behaviors inside a hydrocyclone, such as the effects of turbulence and the processing vortex core phenomenon [74–76], affect separation performance, they are either very fast compared to the valves or suitable for being time-averaged. Thus, describing the internal hydrocyclone fluid mechanics with static functional relationships is enticing. The slower dynamic effects on hydrocyclone separation performance include wear, erosion, and feed composition [77]. Several theories describe hydrocyclone separation performance, such as the concept of estimating the grade efficiency (G), also called migration probability, which is presented in [78, 79]. Models computing oil droplet trajectories using estimations of the internal flow fields are described in [69, 70], and proved to be a reasonable method of obtaining G. Additionally, [80] defines an accurate model for migration probability using swirl intensity for estimation of the axial, radial, and tangential velocity fields and is also based on oil droplet trajectories. There is an incentive to model the separation performance, specifically to estimate the OiW concentration of the discharged water, as real-time OiW concentration monitors have limitations and might even prove to be unreliable, as described in [81]. However, OiW monitors have great potential for reporting, decision support, and advanced control with the aim to improve PWT [56, 82].

Motivation for Real-Time Oil-in-Water Measurements

Fundamentally, estimation and measurement are valuable in the pursuit of obtaining the true OiW concentration of the discharged water in real-time, and required for some state-of-the-art control solutions, such as in [83]. Additionally, it is important to state that neither estimations nor measurements will yield the true value, as a result of their limitations, imperfections, and accuracies, but they should be reasonably accurate to be considered valuable. A well-established notion of OiW measurements is that they are highly methodology-dependent as different methods are sensitive to different characteristics of oil content, especially for real-time measurements [17, 81]. Previous studies have used real-time OiW measurements, with various degrees of critical opinions of the measured values [56, 81, 84–86]. There is motivation to use real-time OiW concentration monitors to validate model performance.

1.3 Outline of the Papers

This thesis consists of an extended summary followed by the paper contributions. The purpose of the extended summary is to describe the background and motivation of the combined paper contributions. An overview of the paper contributions and how they relate are shown in Fig. 1.5. This section describes the motivation of each paper contribution.

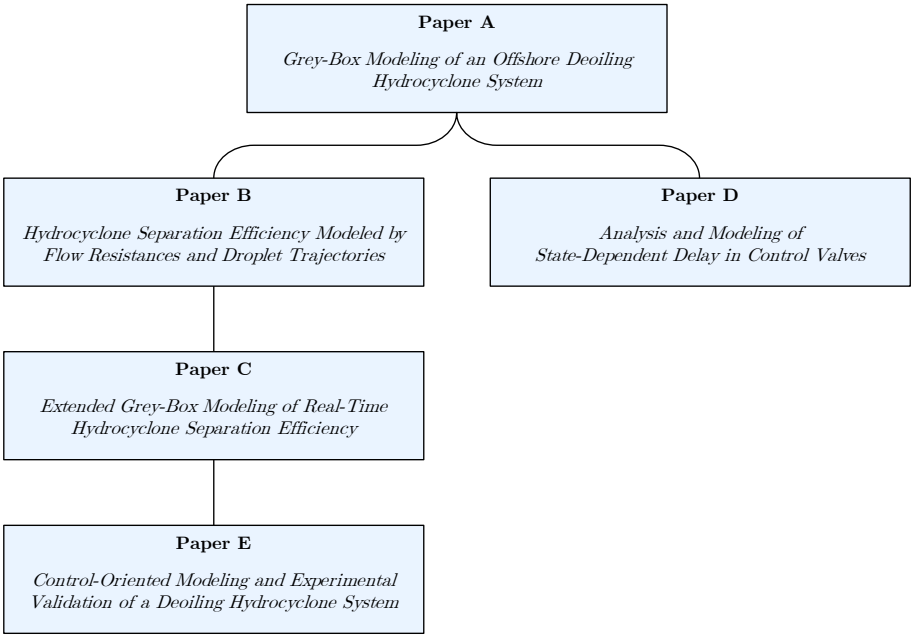

Fig. 1.5: Overview of paper contributions.

1.3.1 Motivation for Paper A [87]

Paper A proposes a model framework that exploits the benefits of using the actual valve opening percentages, such that the dynamics of the valves can be described individually and externally. This paper aims to bridge the gap between how the valves affect pressure drops to how flow rates affect the oil droplet trajectories inside of a hydrocyclone. To achieve this, the hydrocyclone is mathematically decomposed into simpler flow resistances via orifice equations, which proved to be a reasonable approach to model the pressure drops and flow rates of the hydrocyclone. The model was experimentally validated using flow rate and pressure measurements.

1.3.2 Motivation for Papers B [88] and C [89]

Papers B and C describe how Q_u and Q_o can be used to estimate the separation efficiency by evaluating oil droplet trajectories. The modeling of the oil droplet trajectories is inspired from the work in [69, 70]. A key issue thereof is having the axial velocity profile as a scaled polynomial with fixed parameters, which renders the axial velocity profile valid in only the vicinity of the chosen operating F_s. Paper C extends and improves the proposed model. The key improvement is how the axial velocity profile is now solved based on flow rates rather than being fixed. The extended model was benchmarked with the model from Paper B and showed improved prediction performance.

1.3.3 Motivation for Paper D [90]

The hydrocyclone does not accumulate fluid like the separator tank, and with the small volume and high flow rate the residence time inside a hydrocyclone is short. This causes the hydrocyclone dynamics to be much faster than the separator tank, and dominantly determined by the valve speed and characteristics. Paper D investigated an observed non-linear delay phenomenon of the valves. This delay originates from the valve system being a close-loop controlled hysteresis system, such that when the valve system is commanded to change direction, additional output delay is observed. The paper proposed a pin-cart model to predict the actual valve opening given the wanted valve opening.

1.3.4 Motivation for Paper E [91]

As there are several issues related to measuring low OiW concentrations in real-time as stated in [81], an improved testing rig was constructed with redundant OiW monitors to further strengthen the validation of the model proposed in Paper B and C. This paper also investigates the OiW monitors under various conditions. To the authors' knowledge, this is the first time this configuration of four real-time fluorescence-based monitors have been utilized to evaluate hydrocyclone performance. Additionally, this paper combines and elaborates on the work done in Papers A, B, and C.

Chapter 2

Model Framework

This chapter summarizes the modeling approach presented in the Papers A−E. This section defines the proposed model structure of the hydrocyclone system shown in Fig. 1.2, that uses the valves V_u and V_o as controllable inputs, and the pressures P_i, P_{ub}, and P_{ob} as external inputs.

Previous first principles modeling approaches of inline hydrocyclones are presented in [51]. Here, the goal was similar to the proposed methodology of this work; to be used for developing coordinated control solutions by being compatible with holistic separation plant models. A strong example of how separation-based models can be used to improve the total performance of the plant is shown in [52]. Recent promising simulations of deploying sliding mode control on a separation-based hydrocyclone model for controlling C_u is shown in [83].

The proposed model structure of this work is divided into model blocks, where each model block represents a physical mechanism or subsystem of the deoiling hydrocyclone system. The advantages of this approach are primarily to have access to estimated intermediate operational variables, and flexibility by model block selection. The combined deoiling hydrocyclone model is illustrated in Fig. 2.1, and shows the first step of isolating the dynamics of the valves into a model block.

The proposed model of this thesis is designed for MPC, to improve the overall system performance by having access to separation metrics, such as ε_{oil} and G. Thus, the model is designed to seamlessly fit into a higher-level plant model that includes models of the other separation systems, such as three-phase separators, compact gas flotation units, and membrane filtration units. Here the proposed objective is: "Minimize cost while complying with discharge regulations". While the discharge regulations are clearly defined, the cost is entirely up to the operators' economic strategy. The cost could simply be throughput loss. However, as an example, the cost could also be

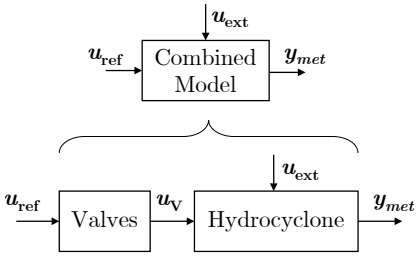

Fig. 2.1: Proposed model structure, with controllable valve opening references (u_{ref}), actual valve openings (u_V), uncontrollable inputs (u_{ext}), and separation performance metrics (y_{met}).

estimated loss of cumulative throughput over the next five years. It is up to the operator how net present value (NPV), and other risks, are weighted in their operational strategy.

The expanded proposed model framework is illustrated in Fig. 2.2, where the valve model block is described in Chapter 5, the virtual flow resistance (VFR) model block is described in Chapter 4, and the oil droplet trajectory (ODT) model block is described in Chapter 3.

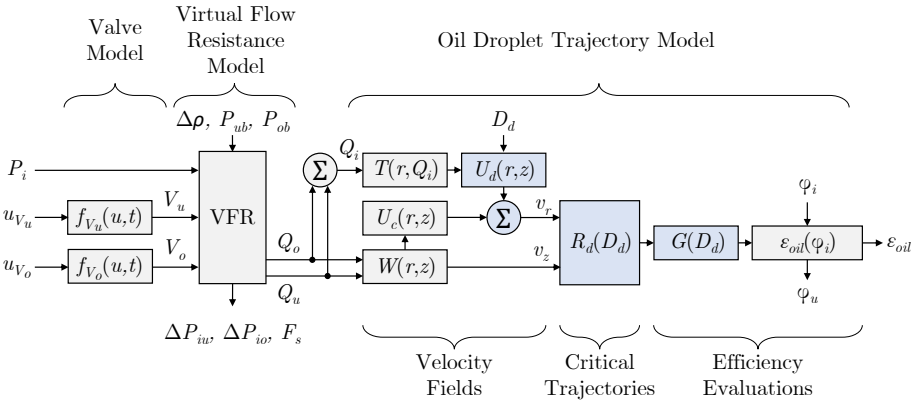

Fig. 2.2: The framework of the proposed control-oriented hydrocyclone model consisting of three main parts: 1. dynamic model of the valves from commanded to actual valve opening, 2. flow rate estimation by a virtual flow resistance model, and 3. efficiency estimation obtained from evaluating oil droplet trajectories. Blue blocks need to be evaluated in a discretized range of droplet diameter (D_d).

The benefit of having access to intermediate variables is similar to having access to the observed states of a system. The intermediate variables are beneficial for providing valuable internal system insight during operation, which specifically can be used in domains such as fault detection and diagnosis (FDD), alarm reasoning, and root-cause analysis.

As the hydrocyclone valves have variations in operational properties, it is only reasonable to assume that the valve model block has to be replaced by a system-specific valve model during offshore implementation of the model. This emphasizes the value in defining the combined model structure, with flexible model blocks that can be interchanged, to represent a specific deoiling hydrocyclone system. The interchangeability also exists for components in the VFR model and the ODT model. This flexibility, to set up a reasonable model for a specific hydrocyclone system, is specifically valuable for control design, preliminary training of machine learning models, and deoiling performance evaluations and analysis.

Chapter 3

Virtual Flow Resistance Model

Common trajectory-based hydrocyclone models require a notion of the flow rates entering and leaving the hydrocyclone, such that the internal spacial velocity fields can be approximated [69, 70, 80, 92, 93]. If an advanced hydrocyclone model is proposed to be incorporated into systems running with PDR control, it is convenient for the model to use the exact same measurements as the ones already used: P_i, P_u, and P_o. Additionally, the measurements of Q_i, Q_u, and Q_o, might be unavailable on an offshore PWT system. As the valve systems are directly actuated by the control, it is also convenient to incorporate the actual valve openings into the model equations, such that the commanded valve openings are inputs to the model. This enables future predictions of performance, given different input strategies of the valve openings.

This chapter summarizes the VFR model proposed in Paper A that aims to model the relationship between the hydrocyclone pressures: P_i, P_u, P_o, P_{ub}, and P_{ob}, and flow rates: Q_i, Q_u, and Q_o.

3.1 Flow Resistance Model Structure

A model of the static relationship between valve openings, pressures, and flow rates are obtained from mathematically decomposing the hydrocyclone into a circuit of virtual flow resistances, as shown in Fig. 3.1.

Each virtual resistance is described by an orifice equation, which provides a system of equations of pressure drops. The pressure drops over the virtual resistances are

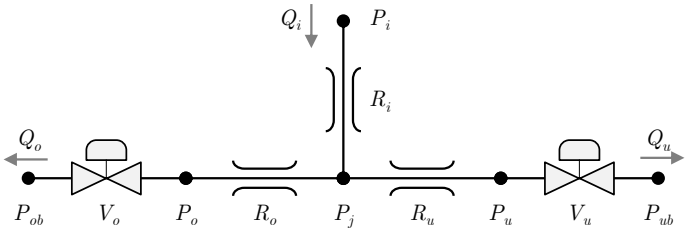

Fig. 3.1: Proposed flow resistance model based on pressure drops over virtual orifices. The virtual pressure (P_j) is not measured, as it is the pressure at a virtual junction. Figure is from Paper E.

$$\Delta P_{ij} = P_i - P_j = \frac{(Q_u + Q_o)^2}{K_i} \,, \tag{3.1}$$

$$\Delta P_{ju} = P_j - P_u = \frac{Q_u^2}{K_u} \,, \tag{3.2}$$

and

$$\Delta P_{jo} = P_j - P_o = \frac{Q_o^2}{K_o} \,, \tag{3.3}$$

where K_i, K_u, and K_o are the inlet, underflow, and overflow flow conductance constants, respectively. As mentioned in Section 1.2.1, valves have great diversity in characteristics, thus, the static valve equation should be chosen based on application. For this work, the valve equations were implemented in the system of equations as

$$P_u - P_{ub} = \frac{Q_u^2}{(K_{V_u} V_u)^2} \,, \tag{3.4}$$

and

$$P_o - P_{ob} = \left(\frac{Q_o}{K_{V_o 1} V_o^{\frac{1}{2}}} \right)^2 + \frac{Q_o^2}{K_{V_o 2}^2} \,, \tag{3.5}$$

where K_{V_u}, $K_{V_o 1}$, and $K_{V_o 2}$ are valve specific flow conductance constants. An experimental data set, containing pressure and flow rate measurements, is required to identify the flow conductance parameters, which can be obtained from laboratory experiments of the specific hydrocyclone or from historic operational data. The VFR model parameters are found by minimizing the error between the model output and the measurements from the data set.

One minimization problem, to find the set of flow conductance parameters ($\mathbf{K}$), is formalized as

$$\underset{\mathbf{K}}{\text{minimize}} \; e_{VFR}(\mathbf{K}) = \sum_{n=1}^{N_{dp}} \left(\left(\frac{Q_{u,n} - \widehat{Q}_{u,n}}{\overline{Q}_u} \right)^2 + \left(\frac{Q_{o,n} - \widehat{Q}_{o,n}}{\overline{Q}_o} \right)^2 + \left(\frac{P_{u,n} - \widehat{P}_{u,n}}{\overline{P}_u} \right)^2 + \left(\frac{P_{o,n} - \widehat{P}_{o,n}}{\overline{P}_o} \right)^2 \right), \tag{3.6}$$

where ($\hat{}$) denotes estimated output, ($\bar{}$) denotes global mean value, N_{dp} is the total number of data points in the experimental data, and n is the data point's index. K_{V_o1} and K_{V_o2} are found from a regression of (3.5) and K_{V_u} is found from a regression of (3.4), using measurements of P_u, P_o, P_{ub}, P_{ob}, Q_u, Q_o, and the actual valve openings of V_u and V_o.

3.2 Experimental Identification and Validation

A hydrocyclone testing rig was used to obtain training data for the model. To represent a wide range of operating conditions in the training data, the valves were coordinated to visit a 21-by-21 grid of the valve openings V_u and V_o. All pressures and flow rates that are included in the VFR model were measured at these grid points, except P_j. The model's prediction performance of Q_u and Q_o is shown in Fig. 3.2.

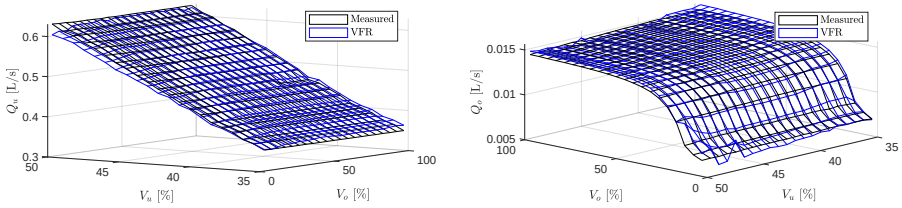

(a) Underflow flow rate

(b) Overflow flow rate

Fig. 3.2: Estimated (blue) and measured flow rate (black) of the training data set that consists of a grid of operating conditions obtained from the hydrocyclone testing rig. Figures are modified from Paper A. © 2017 IEEE.

To validate the model's predictions, a validation test was executed with constant Q_i instead of constant P_i. The estimated F_s can be seen in Fig. 3.3 of the training and the validation data set.

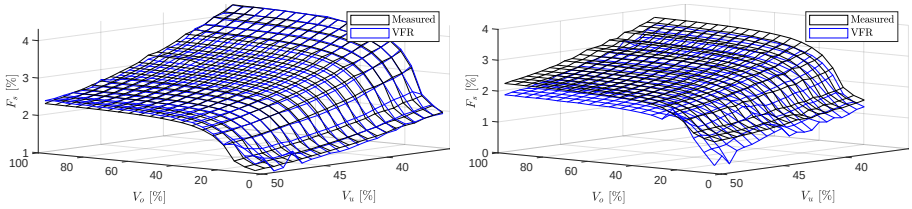

(a) Training **(b)** Validation

Fig. 3.3: Estimated (blue) and measured F_s (black) from training and validation data set that both consist of a grid of operating conditions obtained from the hydrocyclone testing rig. The training data set has operating conditions with constant inlet pressure and the validation data set has operating conditions with constant inlet flow rate. Figures are modified from Paper A. © 2017 IEEE.

3.3 Conclusion

A VFR model of a deoiling hydrocyclone, that uses valve openings and pressure measurements, was proposed to obtain estimates of Q_u and Q_o. The VFR model proved to be reasonably accurate in predicting flow rates and pressures of the training and the validation data. One significant disadvantage of the VFR model is that the parameter identification requires data, which might be unavailable or costly to obtain. A method of addressing this disadvantage is to investigate if the parameters can be estimated by an observer in real-time. The largest prediction errors were observed near valve saturation, where at least one of the valves approaches being either fully opened or fully closed. The model is deemed suitable for bridging the gap between the controllable actuators (the valves) and the trajectory-based models that require inputs of Q_u and Q_o.

Chapter 4

Oil Droplet Trajectory Model

This chapter defines the proposed ODT model that estimates G based on Q_u and Q_o, hydrocyclone geometry parameters, and fluid properties. The proposed model is designed to enable the control solution to estimate or predict the separation performance, given current or future actions. The idea for the proposed ODT model was first shown in Paper A and was inspired by ODT models from [69, 70]. The first presented ODT model combined with the VFR model is presented in Paper B. The proposed ODT was extended to yield better prediction performance in Paper C, and validated using real-time OiW measurements in Paper E. The proposed ODT model consists of the following steps:

1. Estimate continuous phase velocity fields ($[W, U_c, T]$).
2. Estimate dispersed phase settling velocity (U_d).
3. Compute a set of critical droplet trajectory starting locations (R_d).
4. Estimate G.
5. Estimate ε_{oil}.

The remaining of this chapter will summarize each of the steps. The geometry used in the proposed ODT model is shown in Fig. 4.1 with the specifications listed in Paper E.

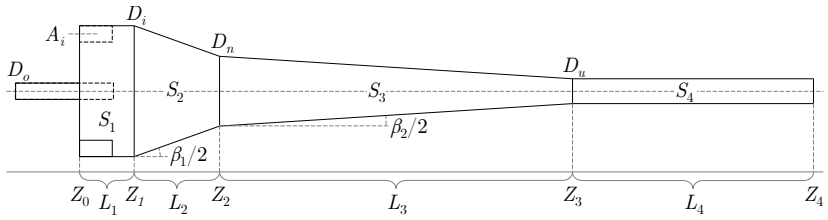

Fig. 4.1: Hydrocyclone geometry with diameters D, segments S, segment lengths L, cone angles β, axial locations Z, and inlet area A_i. Figure is from Paper E.

4.1 Velocity Fields

This section proposes a method to approximate the three spacial velocity fields inside the hydrocyclone segments S_{3-4}, as seen in Fig. 4.1. The velocity fields are defined in a radial-axial (r, z)-coordinate system with $z = 0$ at Z_2 and $r = 0$ at the hydrocyclone center axis, cf. Fig 4.1. The three spacial velocity fields are assumed to be time-averaged, time-invariant, and rotationally symmetric, with the implications discussed in Paper E.

4.1.1 Tangential Velocity Field

Tangential speed (T) is modeled by a modified Helmholz law from [70], such that

$$T(r) = \frac{v_i \alpha (2R_z(0))^n}{r^n}, \tag{4.1}$$

where $n \in [-1, 1]$ is a constant that describes how forced or free the vortex is, α is a velocity loss coefficient due to imperfection, $R_z(0)$ is the inner wall radius at $z = 0$, and v_i is inlet speed defined by

$$v_i = \frac{4\frac{Q_i}{2}}{\pi D_i^2}\ . \tag{4.2}$$

This definition of v_i is specific for a hydrocyclone with two symmetrically placed tangential inlets using the equivalent inlet diameter (D_i).

4.1.2 Axial Velocity Field

The axial velocity is either modeled as a constant velocity distribution as in [70], which is valid near the designed F_s, or solved based on fluid flow which is more versatile, but requires the knowledge of Q_u and Q_o. As the

two flow rates are provided by the VFR model, the axial velocity profile (Y) in normalized radius $\hat{r} = r/R_z(z)$ is defined as the polynomial

$$Y(\hat{r}) = \theta_1 + \theta_2\hat{r} + \theta_3\hat{r}^2 + \theta_4\hat{r}^3 \,, \tag{4.3}$$

which is solved based on four constraints:

1. Maximum axial velocity at the inner wall:

$$\left.\frac{dY(\hat{r})}{d\hat{r}}\right|_{\hat{r}=1} = 0 \,. \tag{4.4}$$

2. Minimum axial velocity at the center axis:

$$\left.\frac{dY(\hat{r})}{d\hat{r}}\right|_{\hat{r}=0} = 0 \,. \tag{4.5}$$

3. Volume balance of the forward axial flow:

$$Q_{for} = 2\pi \int_{\hat{R}_L}^{1} Y(\hat{r})\hat{r}d\hat{r} \,. \tag{4.6}$$

4. Volume balance of the reverse axial flow:

$$Q_{rev} = -2\pi \int_{0}^{\hat{R}_L} Y(\hat{r})\hat{r}d\hat{r} \,. \tag{4.7}$$

The four constraints are evaluated at Z_2 and governed by the following definitions:

- Definition of locus of zero axial velocity:

$$Y\left(\hat{R}_L\right) = 0 \,. \tag{4.8}$$

- Definition of forward going flow outside $\hat{R}_L$:

$$Q_{for} = Q_i + Q_r = (1 + R_R)(Q_u + Q_o) \,. \tag{4.9}$$

- Definition of reverse going flow inside $\hat{R}_L$:

$$Q_{rev} = Q_o + Q_r = (1 + R_R)Q_o + R_R Q_u \,. \tag{4.10}$$

The locus of zero axial velocity ($R_L(z)$) describes the radius where the axial velocity is zero, as a function of z [94]. The phenomenon of a recirculation flow (Q_r) illustrated by the grey region in Fig. 4.2 and short circuit flow are described in [61, 94, 95].

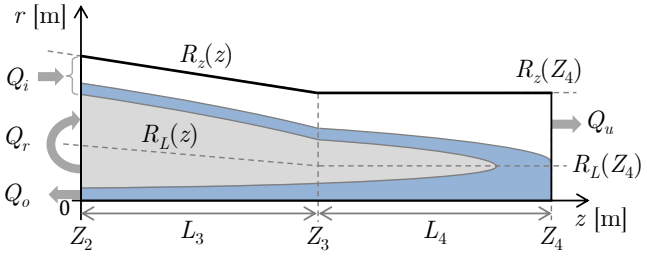

Fig. 4.2: Illustration of the defined flow regions in S_{3-4}. The fluid moves to the right above R_L and to the left below R_L. At Z_2, the flow rate above R_L is $Q_{for} = Q_i + Q_r$ and the flow rate below R_L is $Q_{rev} = Q_r + Q_o$. Both Q_{for} and Q_{rev} are derived from the flow rate through the axial cross-section at Z_2. Figure is from Paper E.

In summary, (4.4)−(4.10) are a set of equations that are solved for the four unknowns in (4.3) given the knowledge of Q_u and Q_o. The flow rate definitions of Q_{for} in (4.9) and Q_{rev} in (4.10) are illustrated in Fig. 4.2 at Z_2.

The recirculation rate, $R_R = Q_r/Q_i$, describes how Q_r scales with Q_i, which is a phenomenon described in [61, 70, 94]. This work uses $R_R = 0.02$, which is achieved from matching Y from (4.3) to the experimentally obtained Y from [70]. In perspective, R_R describes the size of the grey recirculation zone in Fig. 4.2. Even though, R_R is calculated based on measurements from [70], it is likely that the model benefits of identifying R_R based on measurements from the given hydrocyclone or based on CFD simulations. To describe how Q_o and Q_r eventually crosses R_L, the average speed across the locus is defined as

$$v_L = \frac{Q_{rev}}{A_L} \,, \tag{4.11}$$

where

$$A_L = \pi \hat{R}_L \left(L_3 \left(\frac{D_n + D_u}{2} \right) + L_4 D_u \right) \,, \tag{4.12}$$

is the total area of the envelope of zero axial velocity, consisting of a conical and a cylindrical segment.

The axial velocity at all points inside S_{3-4} is defined as

$$W(r,z) = W_s(z) \frac{Y\left(\frac{r}{R_z(z)}\right)}{R_z^2(z)} \,, \tag{4.13}$$

where the effect of how flow is drained across the locus is modeled by axial speed scale $W_s \in [0,1]$ defined as

$$W_s(z) = 1 - \frac{|v_L 2\pi \int_0^z R_L(\check{z})\, d\check{z}|}{Q_{for}} \,. \tag{4.14}$$

All dispersed oil droplets are assumed to have the same axial and tangential velocity as the carrying phase.

4.1.3 Radial Velocity Field

The radial velocity field of the carrying phase (U_c) is defined as a sum of two effects: radial velocity due to conical inner wall (U_w), as described in [32], and radial velocity due to draining across the locus of zero axial velocity (U_L), such that

$$U_c(r,z) = U_w(r,z) + U_L(r,z)\ , \tag{4.15}$$

where

$$U_w(r,z) = \frac{-r}{R_z(z)} W(r,z) \tan\left(\frac{\beta_2}{2}\right), \tag{4.16}$$

and

$$U_L(r,z) = -v_L \frac{R_L}{r} \frac{\int_{\check{r}}^{1} 2\pi\check{r}Y(\check{r})d\check{r}}{Q_{for}}\ . \tag{4.17}$$

It should be noted that $U_w = 0$ in S_4, as the inner wall is cylindrical in this segment. The only velocity difference between carrying and dispersed phase is assumed to be the terminal settling speed (U_d) derived from Stokes law

$$U_d(r,D_d) = -\frac{\Delta\rho D_d^2 T(r)^2}{18\mu r}\ , \tag{4.18}$$

where μ is the dynamic viscosity of water and $\Delta\rho$ is the density difference between the water and oil. The assumption that U_d is the only velocity difference between the phases is a fair assumption according to literature [70, 75]. This assumption is thoroughly discussed in [39, 96].

4.2 Trajectories

The three defined velocity fields enable oil droplet trajectories to be computed starting from any point inside S_{3-4}. All three velocity fields are assumed to be time-averaged, such that T only provides information about the number of revolutions a droplet undertakes. As the number of revolutions is not important for evaluating a droplet's termination state, the oil droplet trajectories are calculated in the (r,z)-plane, with the velocities

$$\begin{bmatrix} v_r \\ v_z \end{bmatrix} = \begin{bmatrix} U_c(r,z) + U_d(r,D_d) \\ W(r,z) \end{bmatrix}\ . \tag{4.19}$$

4.2.1 Critical Droplet Trajectory

One inconvenient computational approach to evaluate the termination state of a droplet, with diameter D_d, is to calculate trajectories starting from the inlet flow until the trajectories terminate by satisfying either $r \leq R_L(z)$ or $z \geq Z_4$ by stepping forward in time. To reduce the computation load, only one critical droplet trajectory is evaluated for a droplet with diameter D_d starting the trajectory from $(R_L(Z_4), Z_4)$ and stepping backward in time, until the trajectory terminates when $r \geq R_z(z)$ or $z \leq Z_2$. An example of a critical droplet trajectory is shown in Fig. 4.3.

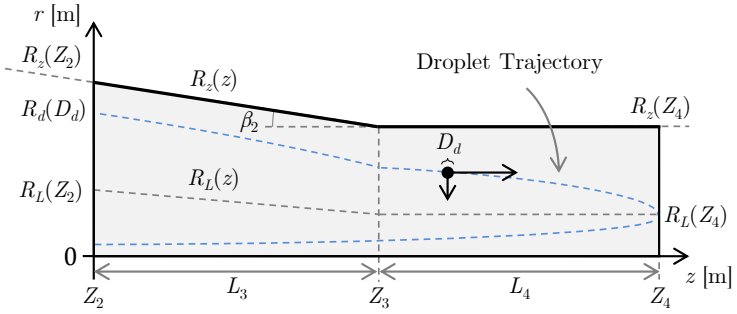

Fig. 4.3: Illustration of a critical droplet trajectory inside S_{3-4}. Figure is from Paper E.

The assessments about whether a droplet becomes separated or not are based on where the critical droplet trajectory terminates. If the critical trajectory terminates at the inner wall, the droplet is so large that it does not matter where it would have started at the inlet; it will always reach the locus before reaching the underflow. If the critical trajectory terminated at Z_2, as in Fig. 4.3, the radius at termination is stored in $R_d(D_d)$, as this radius is needed for evaluating G.

4.2.2 Grade Efficiency

In summary, a droplet with diameter D_d is assumed to leave through the overflow if it enters S_3 inside $R_d(D_d)$ and assumed to leave through the underflow if it enters S_3 outside $R_d(D_d)$. With the assumption that the droplets are uniformly distributed in volume, the flow rate of Y between $R_d(D_d)$ and $R_z(0)$ is compared to Q_i, such that the separation chance of a droplet with diameter D_d becomes

$$G(D_d) = 1 - \frac{2\pi \int_{\frac{R_d(D_d)}{R_z(0)}}^{1} \hat{r} Y(\hat{r}) d\hat{r}}{Q_i} . \tag{4.20}$$

An illustration of the typically S-shaped G is shown in Fig. 4.4 [97, 98]. The model's trajectory estimation is not affected by randomness from turbulence nor the short-circuit flow phenomenon, where oil creeps along the boundary layer of the hydrocyclone inner wall directly to the underflow [61, 99]. As a result, the estimation of G reaches 100%, as shown in Fig. 4.4.

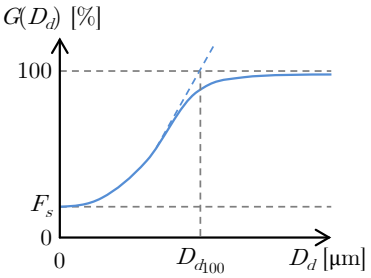

Fig. 4.4: Illustration of $G(D_d)$. When D_d approaches zero, the only oil content that is removed corresponds to F_s. Generally, $G(D_d)$ increases with D_d. The full blue line approaches 100%. The model's prediction is illustrated by the blue dashed line, that diverges from the real system as short-circuit flow and random-walks from turbulence and Brownian motion, are not accounted for. $D_{d_{100}}$ is the smallest droplet with a 100% chance of being separated.

4.3 Separation Efficiency

To estimate ε_{oil}, the volumetric inlet droplet size distribution ϕ_i can be used, such that

$$\varepsilon_{oil} = \int_0^\infty G(D_d)\phi_i(D_d)dD_d \, . \tag{4.21}$$

It should be noted that the inlet droplet sizes are mainly distributed in $5-60$µm [30, 70]. To reduce computation load, the knowledge of $G(D_d) = 100\% \; \forall \; D_d > D_{d_{100}}$ renders (4.21) into two terms, such that

$$\varepsilon_{oil} = \int_0^{D_{d_{100}}} G(D_d)\phi_i(D_d)dD_d + \int_{D_{d_{100}}}^\infty \phi_i(D_d)dD_d \, . \tag{4.22}$$

As the trajectories are computed in a range with discrete droplet sizes, the integral is practically implemented as a sum of vector elements,

$$\varepsilon_{oil} = \sum_{n=1}^{N_{100}} G(n)\phi_i(n) + \sum_{n=N_{100}+1}^{N} \phi_i(n) \, , \tag{4.23}$$

where N is the total number of droplet diameters, $G(n)$ and $\phi_i(n)$ are vectors wherein each element, indexed by n, corresponds to a specific droplet diameter, and $G(N_{100}) = 100\%$. The distribution and resolution of the included

droplet diameters are chosen based on a balance between model accuracy and computational load. A good practice is to choose N, such that increasing N further yields insignificant estimation accuracy.

4.4 Conclusion

Given the two flow rates Q_u and Q_o, the proposed ODT model provides an estimate of ε_{oil}. The model updates the hydrocyclone velocity fields based on the flow rate. If ϕ_i is unknown, G can be used as a separation performance indicator. The computational load mainly consist of computing the set of droplet trajectories backward in time numerically. With this approach, the total number of chosen droplet diameters and the time step size of the trajectory solver must be chosen according to a balance between model accuracy and computational load. The ODT model estimates intermediate flow variables such as velocity fields and oil droplet trajectories that can be used for investigatory purposes. The internal flow conditions can also be used for decision support, predicting possible fault scenarios, or to simply explain why low efficiency was achieved. The performance of the ODT model is evaluated and validated in Chapter 6.

Chapter 5

Inherent Delay of Control Valves

Control valves are ubiquitous in various process industries, where they serve as a fundamental technology to manipulate fluid flows and pressures. Even though they have been extensively used, control valve problems still account for 32% of cases where process controllers have been classified as having "poor" or "fair" performance, as estimated by [100]. As good control valve performance often directly relate to economical benefits, there is an incentive to account for various unwanted non-linear features, such as dead-time, hysteresis, stiction, backlash, and deadband [101–103]. This chapter proposes a method to model control valves with inherent internal position controllers. Specifically, the observed input-output delay that is dependent on prior actuation of the control valve, caused by unintended physical effects, is analyzed and modeled. In this chapter, the closed-loop valve system of the overflow valve, as shown in Fig. 5.1, is investigated.

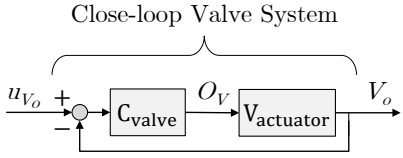

Fig. 5.1: Illustration of the closed-loop control diagram of the overflow valve, where an internal position controller (C_{valve}) actuates the valve piston ($V_{actuator}$) towards the input reference (u_{V_o}), using measurements of the actual valve position (V_o). O_V is the unmeasured output of the internal valve controller.

The first assumptions of this closed-loop system are that $u_{V_o} \in [0, 1]$ and $V_o \in [0, 1]$, which classifies this system to be single-input single-output (SISO)

and bounded-input bounded-output (BIBO). Additionally, the system has a steady-state gain of 1 as a result of the internal valve controller.

5.1 Delay Investigation

The delay was investigated by performing an experiment where u_{V_o} is designed as series of random values with random hold time. The tested valve is a Bürkert 8802-GD-I pneumatic valve system. The step responses of V_o were collected, as shown in Fig. 5.2.

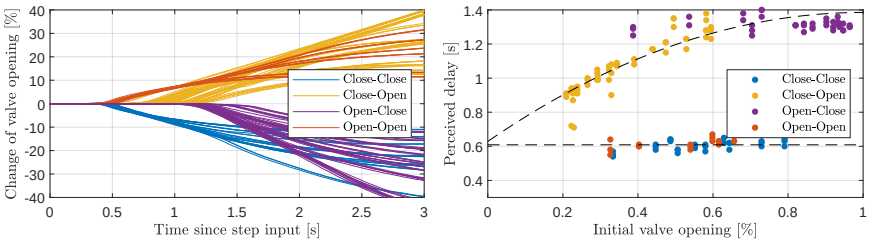

(a) Collection of step responses. Each step response is offset to start from 0% and time-shifted to start from 0s for illustration purposes.

(b) Input-output delay of each step response as function of initial valve position, where this delay is defined as the time it takes the output to change 2%.

Fig. 5.2: Step responses from a series of random steps. The step responses are dependent on their previous step as indicated by color, e.g., a blue response is two consecutive declining steps, a red response is two consecutive increasing steps. Figures are modified from Paper D.

From the collection of step responses, the perceived input-output delay is clearly shorter when the valve is commanded in the same direction as their previous step, as shown with blue and red in Fig. 5.2. When the valve is commanded in a different direction than its previous step, the delay is longer, as shown with yellow and purple in Fig. 5.2. Additionally, the length of the longer delay is dependent on the initial position of the valve, as shown in Fig. 5.2b. This is attributed to the physical configuration of the tested pneumatic valve, specifically the orientation of its spring load and air feed.

5.2 Pin-Cart Model I

To model this delay phenomenon observed in Section 5.1, two pin-cart type model structures are proposed. This section summarizes the pin-cart model I. The concept of the pin-cart type model is illustrated in Fig. 5.3. Firstly, the valve opening error is defined as

$$e(k) = u_{V_o}(k) - V_o(k). \tag{5.1}$$

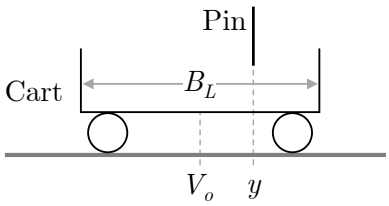

Fig. 5.3: Illustration of the pin-cart model with pin position (y), cart position (V_o), and cart width (B_L). Figure is modified from Paper D.

The change of pin position ($\Delta y(k)$) is defined to have a minimum and maximum speed, such that

$$\Delta y(k) = \text{sgn}(e) \cdot \max\left(|P_k \cdot e|, \Delta y_{min}\right), \tag{5.2}$$

where $\Delta y \in [-\Delta y_{max}, \Delta y_{max}]$ and P_k is the proportional gain of an internal controller. $y(k)$ is updated as

$$y(k+1) = y(k) + \Delta y(k). \tag{5.3}$$

The cart position is updated as

$$V_o(k+1) = \begin{cases} y(k+1) - \frac{B_L}{2}, & \text{if } y(k+1) - V_o(k) \geq \frac{B_L}{2} \\ y(k+1) + \frac{B_L}{2}, & \text{if } y(k+1) - V_o(k) \leq \frac{-B_L}{2} \\ V_o(k), & \text{otherwise} \end{cases}. \tag{5.4}$$

In summary, this model has two tuning parameters P_k and B_L. When the valve changes direction, the pin has to travel to the other side of the cart, which emulates a longer input-output delay.

5.3 Pin-Cart Model II

The pin-cart model II is designed to account for how the long delay when changing direction is dependent on the initial valve opening. This is done by assigning a position-dependent pin speed, when the pin is not engaged with the cart's sides, such that

$$\Delta y(k) = \text{sgn}(e) \cdot (a_p V_o(k)^2 + b_p V_o(k) + c_p)^{-1}, \tag{5.5}$$

where a_p, b_p, and c_p are coefficients of the second-order polynomial shown in Fig. 5.2b. In summary, this model emulates position-depended delay when changing direction, at the cost of having to identify a_p, b_p, and c_p.

5.4 Validation and Comparison

The pin-cart models I and II were evaluated using another experiment where the valve was continuously actuated. The performance was compared with modelless, delayed modelless, first-order-plus-dead-time (FOPDT), and the state-of-the-art stiction model with dead-time as defined in [72], and summarized in Table 5.1. The compared metrics are the number of free parameters (Np), the mean average error (MAE), the filtered mean average error (MAE_f), the coefficient of determination (R^2), the sum of squared error (SSE), and the relative sum of squared error (SSE_r).

Table 5.1: Valve model performance. Table is modified from Paper D.

Model	**Np**	**MAE**	**MAE_f**	R^2	**SSE**	**SSE_r**
Modelless*	0	1.106%	1.084%	99.62%	14.37	100 %
Delayed Modelless*	1	0.876%	0.858%	99.84%	5.917	41.15%
FOPDT	2	0.869%	0.852%	99.85%	5.770	40.15%
Stiction	3	0.881%	0.864%	99.84%	5.914	41.15%
Pin-cart I	3	0.843%	0.825%	99.86%	5.483	38.16%
Pin-cart II**	7	0.731%	0.711%	99.89%	4.284	29.80%

* This model is a gain of 1, using the input as an estimation of the output.
** $B_L = 1$ and not considered a parameter for this model.

From first observation, it is evident that the error decreases with the number of parameters. This emphasizes the trade-off between accuracy and model simplicity. Even though the pin-cart model II has the least error, it also has the most parameters. The model performance is illustrated in Fig. 5.4.

The 8s time-window has a relatively aggressive actuation of the valve, which is where the performance differences between the valve models are largest. In Fig. 5.4, it is observed that the pin-cart model II can follow the measured position relatively well, as opposed to the three other models. As the model with most parameters performs the best, there is no obvious best choice of dynamical valve model, and this choice must be made depending on the objectives and limitations of the application the model is deployed in.

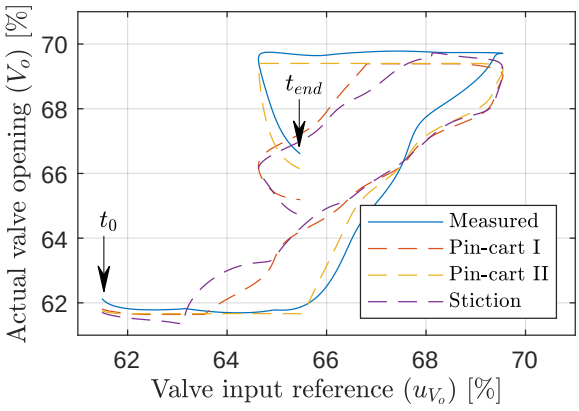

Fig. 5.4: Valve input and output during 8s of the continuously actuated valve experiment. Measured (blue) and estimated (dashed lines) start at the lower left corner, as indicated with t_0, proceed to the right as time goes on, and ends in the center, as indicated with t_{end}.

5.5 Conclusion

As valves are physical systems with undesired intrinsic mechanical properties, it is not a question of if they exhibit delay, but rather a question of how significant the delay is. A dynamic valve model is proposed that exerts opening-dependent input-output delay when changing direction successfully. The proposed pin-cart model includes parameters that directly link to observable valve behaviors, which enables the parameters to be conveniently identified. However, the proposed pin-cart model II requires a set of step responses to identify the opening-dependent delay when changing direction. The pin-cart models can be implemented in larger process models with the purpose of achieving higher accuracy and precision, at the cost of having to identify the valve models' parameters.

Ongoing and future work includes investigations into applying the pin-cart models to other models and systems, such as recurrent neural network (RNN), to describe a reluctance, or delay to change opinion or state.

Chapter 6

Validation of Deoiling Performance

This chapter will address the challenges and findings from validating the proposed model structure using real-time fluorescence-based OiW monitors. To experimentally validate the performance of the proposed modeling methodology, various sensors and monitors have been utilized to measure fluid properties at key locations on a scaled pilot plant. As the proposed model has a modular design, as shown in Fig. 2.2, a list of intermediate flow parameters is estimated by the model, where each model block essentially deserves to be validated. This chapter is organized as follows: first, a brief description of the used experimental hydrocyclone testing facility followed by a description of the challenges of testing with two-phase dispersions. And lastly, the estimations from the proposed model is compared to the measured hydrocyclone separation performance from experiments.

6.1 Hydrocyclone Testing Facility

The validations of the model have been executed on two different generations of the same scaled pilot plant, where Paper A, C, and D include experiments executed on the first generation, and Paper E includes experiments from the second generation. The second generation plant was designed and constructed to address and reduce the effects associated with two-phase dispersions.

The plant was initially constructed to investigate effects of slugging [104] and potential advanced control solutions to reduce the negative effects of slugging [105]. In recent years the pilot plant have been used for investigating and benchmarking OiW monitors [81], membrane filtration for PWT [31], and

hydrocyclones in this work. In summary, the scaled pilot plant includes:

- **Supply tank** with three compartments: water, oil, and mixture, from where pumps supply and valves direct fluid to other subsystems.
- **Pipeline riser subsystem** with 30m horizontal, 12m inclination, and 6m vertical pipes to emulate conditions for slugging flow. This subsystem includes a topside control valve, pressure and flow rate transmitters.
- **Separator tank subsystem** includes a pressurized separator tank, an acrylic transparent separator tank, and associated control valves. This subsystem includes level, flow rate, and pressure transmitters.
- **Hydrocyclone subsystem** with two industrial Vortoil hydrocyclones, an acrylic transparent hydrocyclone, and four slots for custom mini-hydrocyclones, with associated control valves. This subsystem includes flow rate, and pressure transmitters.

The descriptions of the instrumentation are listed in Table 6.1.

Table 6.1: Overview of actuators and sensors.

Symbol	Description	Type	Unit
P_{sep}	Separator pressure	Siemens Sitrans P200	bar
P_i	Hydrocyclone inlet pressure		
P_u	Hydrocyclone underflow pressure		
P_o	Hydrocyclone overflow pressure		
P_{ub}	Hydrocyclone underflow back pressure		
P_{ob}	Hydrocyclone overflow back pressure		
Q_{in}	Separator inlet flow rate	Rosemount 8732 Electromagnetic flow meter	kg/s
Q_i	Hydrocyclone inlet flow rate	Bailey Fischer Porter 10DX4311C Electromagnetic flow meter	L/s
Q_u	Hydrocyclone underflow flow rate		
Q_o	Hydrocyclone overflow flow rate	Micro-Motion Coriolis Elite (CMFS010) Coriolis flow meter	kg/s
V_{gas}	Separator gas valve	Bürkert 8626 mass flow controller	–
V_{top}	Topside choke valve	Bürkert 8802-GD-I pneumatic valve systems	–
V_{oil}	Separator oil valve		–
V_i	Hydrocyclone inlet valve		–
V_u	Hydrocyclone underflow flow rate		–
V_o	Hydrocyclone overflow flow rate		–
WP	Water pump	Grundfos CRNE 5-9 centrifugal pump	–
$Mixers$	Supply tank stirrers	Milton Roy Mixing HELISEM VRP3051S90	–

Two primary OiW monitor types have been investigated for measuring oil droplet size and OiW concentration. The microscopy-based Jorin ViPA was used to measure oil droplet sizes, based on estimating an average Ferret diameter. The fluorescence-based Turner Design TD-4100XDC was used to measure OiW concentration, based on the aromatic oil content in the OiW

mixture. Promising preliminary results obtained from the two types of monitors in [84] was later revealed in [81] to be more intricate and interdependent than conclusive, especially how the calibration of the microscopy monitor only allows valid measurements in a narrow range of droplet sizes. The hydrocyclone testing facility was later upgraded to reduce the unwanted effects that the system has on the measured OiW concentration.

6.1.1 Hydrocyclone Sidestream Upgrade

The pilot plant including the modified hydrocyclone subsystem is shown in Fig. 6.1.

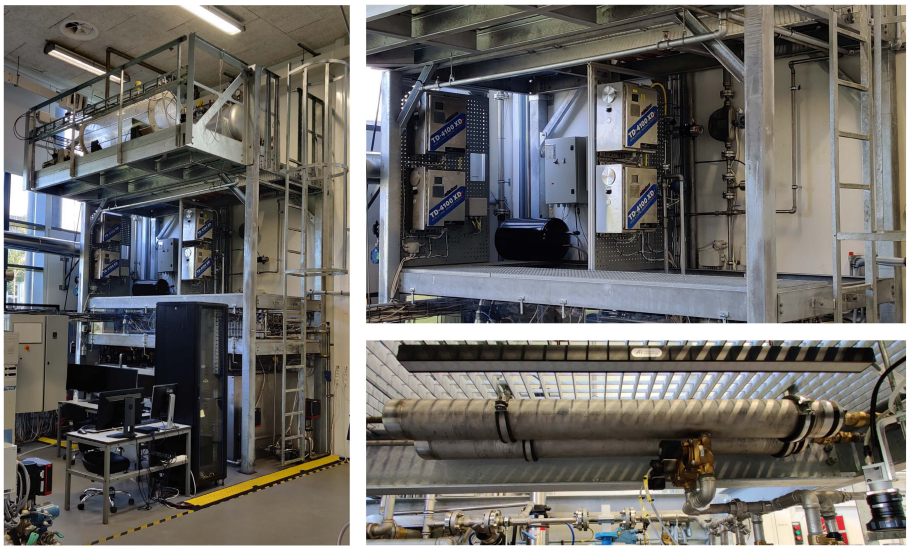

Fig. 6.1: Photo of the pilot plant, with left: the pilot plant, top right: the four OiW monitors located at the hydrocyclone sidestreams, and bottom right: the hydrocyclone liners.

The hydrocyclone subsystem was modified to accommodate more reliable OiW concentration measurements by:

- Reducing fluid travel length between sample extraction and the OiW monitors' sampling points.
- Including two OiW monitors on each sidestream for measurement redundancy.
- Sampling from vertical pipe section to reduce stratification at the sampling point.

- Maintaining constant sidestream flow rate.

The modified pipeline and instrumentation diagram of the upgraded hydrocyclone subsystem is shown in Fig. 6.2.

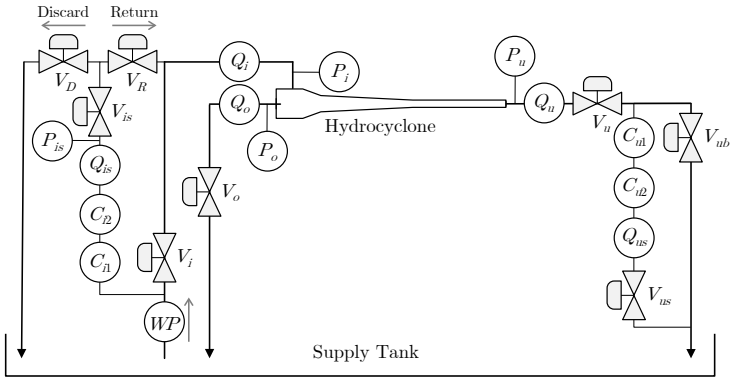

Fig. 6.2: Pipeline and instrumentation diagram of the hydrocyclone subsystem, where C_{i1} and C_{i1} are the inlet OiW monitors, C_{u1} and C_{u2} are the underflow OiW monitors, Q_{is} and Q_{us} are the sidestream flow rates, V_{is} and V_{us} are the sidestream control valves, V_D and V_R are the discard and return valves, V_{ub} is the underflow back pressure valve, and P_{is} is the inlet sidestream pressure. Figure is modified from Paper E.

The sidestreams were constructed with the instrumentation listed in Table 6.2.

Table 6.2: Overview of actuators and sensors.

Symbol	Description	Type	Unit
P_{is}	Inlet sidestream pressure	Siemens Sitrans P200	bar
Q_{is}	Inlet sidestream flow rate	Micro-Motion Coriolis Elite (CMFS010) Coriolis flow meter	kg/s
Q_{us}	Underflow sidestream flow rate	Rosemount 8711 Electromagnetic flow meter	L/s
V_{is}	Inlet sidestream valve	Bürkert 8802-GD-I pneumatic valve systems	–
V_{us}	Underflow sidestream valve		–
C_{i1} C_{i2} C_{u1} C_{u2}	Inlet and underflow sidestream OiW concentrations	Turner Design TD-4100XDC fluorescence-based OiW monitors	ppm

6.2 OiW Mixture Challenges for Real-Time Benchmarks

A general and comprehensive overview of the issues related to measuring OiW concentration using fluorometry is described in detail in [81]. The basic principle of the selected fluorescence-based OiW monitors is based on exciting the mixture in a view cell with light, which will be absorbed by the mixture and emitted back at a lower wavelength, where a light detector records and outputs relative fluorescence units (RFU). This is a convenient method for measuring OiW concentration as it is sensitive to the aromatic oil content and not to water. Four fluorescence-based OiW monitors are calibrated to provide redundant measurements at both the inlet and underflow, with obtained calibration curves shown in Fig. 6.3.

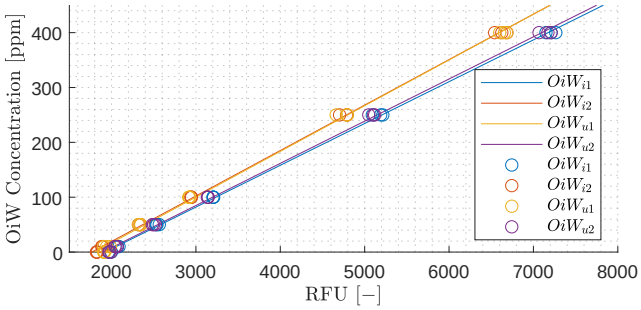

Fig. 6.3: Linear RFU to ppm calibration curves and injected OiW samples of known concentration used to identify them. Figure is from Paper E.

As the obtained calibration curves translate RFU into ppm, their individual RFU readings are allowed to be different, as long as the OiW monitors output the same ppm value for the same OiW sample. Paper E executed experiments to investigate the magnitude of several unwanted effects on the measured OiW. This includes:

- Running the system with a known OiW concentration for extended periods of time. These spanned from changes over a few minutes to daily changes.
- Running the system with closed overflow, to eliminate separation by hydrocyclone, such that inlet and underflow OiW concentrations should be similar.
- Continuously switching between using the hydrocyclone and entirely bypassing the hydrocyclone via a hose from inlet to underflow.

- Running the system while switching between fully open and fully closed V_o, to observe the largest difference in separation efficiency.
- Physically switching two monitors to differentiate position-dependent and monitor-dependent effects.
- Reinjecting known concentrations several days after initial calibration.

Even though two of the OiW monitors were physically switched, they agree in pairs, such that the two inlet OiW monitors agree and the two underflow OiW monitors agree. Therefore, it was concluded that the majority of the effects are caused by a combination of system effects, which are listed and discussed in the following subsection.

6.2.1 System Mixture Challenges

Paper E lists effects that were considered to affect the OiW measurements in the experimental setup other than the separation effects of the hydrocyclone. These effects are suspected of causing the measured and actual OiW concentration to diverge. The effects for the hydrocyclone flow loop are:

- Oil accumulating or being freed from surfaces.
- Oil accumulating or being freed from dead volumes.
- Fouling and cleaning of the OiW monitors' view cell.
- The natural separation versus forced mixing in the supply tank.
- The effects of using T-junctions as sidestream sampling probes.
- Varying shearing causing variations in droplet size distribution.
- Contamination and microbiological growth.

The understanding of these effects and at what time scale they occur are essential for reasonable validation of separation-based hydrocyclone models. Experimental investigation showed that that the hydrocyclone flow loop needed to recirculate and stir the mixture, for up to eight hours before running OiW concentration benchmarking experiments, to allow long-term effects to reach equilibrium. Experiments also revealed an OiW concentration bias between the inlet and underflow OiW monitors, which is likely caused by the different states of fouling the OiW monitors' view cells. Cleaning of the view cells, by means of flushing, helped to reduce this bias, and was executed before and after each experiment. While some of the effects were discussed and investigated in Paper E, there is value in investigating other effects in future works to further strengthen the reliability and understanding of the OiW measurements.

6.3 Validation of Separation Performance

This section will compare measurements with the ODT model's estimations of ε_{oil}. The results presented in this section are based on the long grid experiment presented in Paper E. In summary, the long grid experiment actuates V_u and V_o with staircase inputs, such that each point represents steady-state in an 11-by-14 grid of V_u and V_o. The entire experiment is executed with constant pump speed of 100% and constant mixer speed. The steady-state measurements at each point is generated from the average of the last 10s, just before the system advances to the next grid point by stepping one of the valves. The experiment was executed in segments, where each segment has a constant V_u. Each segment includes a period for system initialization and a period of no separation before and after the period of staircase stepping V_o. The initialization served to allow the flows and pressures to reach steady-state, and the no separation periods served to provide periods where all four OiW monitors could be compared.

The ODT model was provided with measurements of Q_u and Q_o to estimate ε_{oil}. As ϕ_i is unknown, the model was provided with a set of distributions, each with different mean droplet size corresponding to the size distribution obtained in [56], where a Jorin ViPA was used to analyze the droplet sizes by microscopy. The droplet size distribution is chosen as a proof of concept but must be provided by either a model of the upstream process or from measurements for future implementation purposes. The measured and estimated ε_{oil} as a function of Q_i is shown in Fig. 6.4b, where each point corresponds to a steady-state point in the V_u-V_o grid.

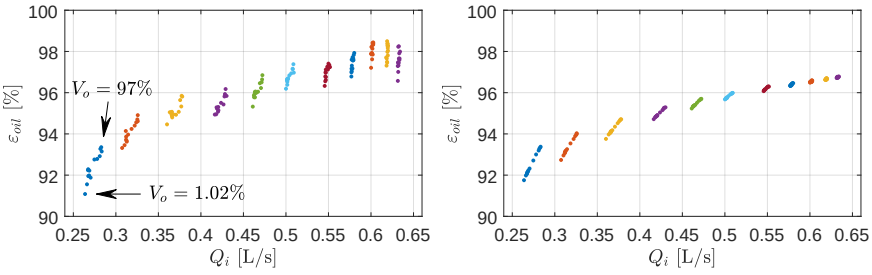

(a) Measured

(b) ODT model

Fig. 6.4: ε_{oil} versus Q_i of steady-state points of the V_u-V_o grid from the experiment. A group of points with the same color indicates steady-state points with the same V_u opening, e.g., the 14 lowest blue points have $V_u = 30\%$ open and the 14 highest purple points have $V_u = 80\%$ open. Within each point group of same color, the left-most point corresponds to $V_o = 1.02\%$ open and the right-most point corresponds to $V_o = 97\%$ open, as indicated by arrows. Generally, ε_{oil} increases with Q_i.

The influence of V_o on both ε_{oil} and Q_i is the span of the points in each

individual color group in Fig. 6.4. An example of this is how V_o can change ε_{oil} from 91−93% and Q_i from 0.26−0.28L/s of the left-most blue color group in which V_u is constant. The measurements and estimation are very similar at low Q_i, and becomes less similar as Q_i increases, where the influence of V_o is significantly lower for the model's estimations. The measurements and the estimations are very similar for how V_u affects ε_{oil} and Q_i. It also appears that the grid points of the measured ε_{oil} are affected by more noise relative to the estimated ε_{oil}. The estimation performance is similar to how ε_{oil} relates to PDR and F_s, as shown in Fig. 6.5.

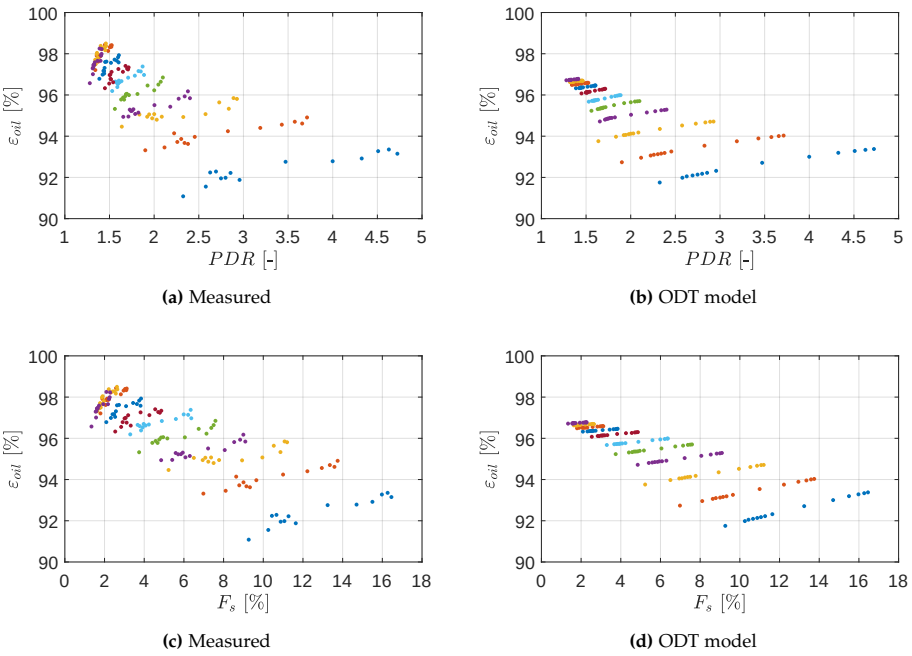

(a) Measured **(b)** ODT model

(c) Measured **(d)** ODT model

Fig. 6.5: ε_{oil} versus PDR and F_s of steady-state points of the V_u-V_o grid from the experiment. A group of points with the same color indicates steady-state points with the same V_u opening, e.g., the 14 lowest blue points have $V_u = 30\%$ open and the 14 highest purple points have $V_u = 80\%$ open. Within each point group of same color, the lowest point corresponds to $V_o = 1.02\%$ open and the highest point corresponds to $V_o = 97\%$ open. Generally, ε_{oil} increases with PDR and F_s within the each group.

It is apparent that one value of PDR does not correspond to one value of ε_{oil}, but rather a range of ε_{oil}, which is captured by both measurements and estimations. The relationship between ε_{oil} and PDR is very similar to the relationship between ε_{oil} or F_s, which complies well with the literature [26, 42, 71], and further validates why it is reasonable to have PDR as a control reference instead of F_s. The strong correlation between PDR and F_s is further emphasized in Fig. 6.6a. The trajectory model proposed by [70] has the

limitation of being fixed to a specific F_s that is uncorrelated with $\hat{R}_L$, which is not the case for the ODT model as seen in 6.6b, where $\hat{R}_L$ is correlated with F_s.

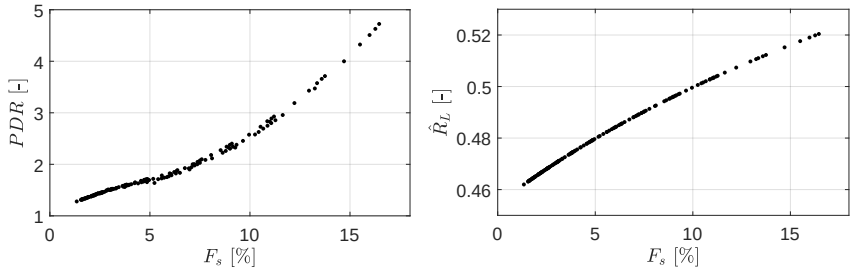

(a) The PDR from measurements pressures plotted against F_s from measured flow rates.

(b) The ODT model's estimation of $\hat{R}_L$ plotted against F_s from measured flow rates.

Fig. 6.6: How F_s relates to PDR and $\hat{R}_L$ at all grid points of the validation experiment.

How the estimated $D_{d_{100}}$ of the ODT model is affected by F_s and Q_i is shown in Fig. 6.7. It is apparent that V_o can affect $D_{d_{100}}$ as shown in 6.7a. However, $D_{d_{100}}$ is significantly more affected by Q_i as seen in Fig. 6.7b.

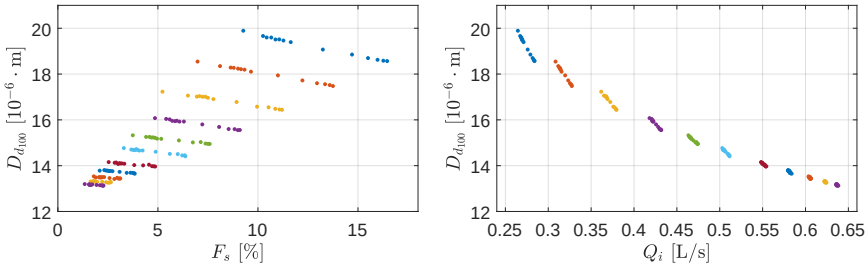

(a) The ODT model's estimation of $D_{d_{100}}$ plotted against F_s from measured flow rates.

(b) The ODT model's estimation of $D_{d_{100}}$ plotted against measured Q_i.

Fig. 6.7: How estimated $D_{d_{100}}$ relates to F_s and Q_i at all grid points of the validation experiment.

An example of the computed trajectories is shown in Fig. 6.8 using the last grid point, where V_u and V_o are the most open. This specific operating condition has $F_s = 2.26\%$, $PDR = 1.41$, $Q_i = 0.634 L/s$, $V_u = 80\%$, and $V_o = 97\%$.

Trajectory A in Fig. 6.8 is computed for a droplet with zero size to have no settling speed from (4.18), such that the trajectory follows the carrying phase. Trajectory C is of the smallest droplet that terminates at the hydrocyclone wall, which is $D_{d_{100}}$, and it is not necessary to compute trajectories of larger droplets in this operating condition. Trajectory B shows an example of a trajectory of a droplet with $D_d < D_{d_{100}}$.

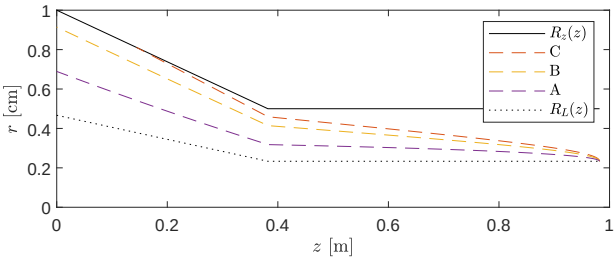

Fig. 6.8: Critical droplet trajectories A, B, and C of three droplets with the diameters 0, 10, and 14µm, respectively. Trajectory A follows the carrying phase, trajectory B reaches and terminates at $z = 0$, and trajectory C is the smallest droplet that reaches $R_z(z)$.

6.4 Conclusion

Several unwanted system effects may cause the measured and actual real-time OiW concentration to diverge. The magnitude of these effects must be minimized to improve the validation of separation-based hydrocyclone models, which require thorough preparations of both system and experiment design. Most of the issues are related to the mixture being a two-phase dispersion that naturally settles and separates in the flow loop. In addition, the low OiW concentration requires the OiW monitors to be very sensitive to oil content, which introduces issues related to low signal to noise ratios. A significant challenge of utilizing high sensitivity involves how various flow conditions affect the OiW measurements, as investigated in [81]. The ODT model was experimentally validated using real-time OiW measurements, which yielded good similarities. The ODT model utilized a mean droplet size of 25µm, as the real ϕ_i was unknown. While the model performance was reasonable, future investigations of how different droplet sizes affect measurements and estimations are valuable and can further strengthen the validation. A significant difference between measurements and estimation was observed, as the estimated ε_{oil} versus Q_i approached a plateau, where measured ε_{oil} versus Q_i reached a global maximum, in Fig. 6.4. However, the measured ε_{oil} global maximum could be a result of system and measurement disturbances rather than being a true global maximum. Additionally, the ODT model predicts the influence of V_o on ε_{oil} to be significantly lower at high Q_i. This discrepancy might be caused by how ϕ_i is constant for the model, but varying in the real system.

In summary, the model is deemed valuable for control design purposes, and other secondary purposes, such as observer-related predictions and generating data sets for learning-based models.

Chapter 7

Closing Remarks

7.1 Conclusion

In this thesis, the challenges to obtain and validate a generalized control-oriented grey-box model of a deoiling hydrocyclone are considered. The main contributions of this work can be summarized to:

- A definition of a versatile control-oriented hydrocyclone model structure with emphasis on practical implementation.
- A proven modeling approach to obtain a control-oriented hydrocyclone model.
- An experimental approach to validate separation-based hydrocyclone models using real-time OiW measurements with emphasis on the challenges and limitations thereof.

A model structure to estimate the hydrocyclone performance metrics, based on commanded valve openings, was proposed in Paper A. To bridge the gap from the actual valve openings to the hydrocyclone flow rates, a VFR model was proposed. The proposed VFR model was experimentally validated and successfully estimated how the pressures relate to the hydrocyclone flow rates. The underflow and overflow valve systems were separated into a dynamic and a static part. The dynamic part translates the electrical valve input into the actual valve opening. The static part is included in the VFR model as an equation that describes how the actual valve opening relates to the pressure drop over the valve and the flow rate through the valve.

To estimate separation efficiency as a hydrocyclone performance metric, a previous ODT model framework from [70] was adapted to be compatible with the VFR model in Paper B. However, this model structure had significant limitations, such as being defined with the assumption that F_s is constant. To

address this, the ODT model was extended and improved in Paper C to be more accurate in a broader range of operating conditions. The revised ODT model solves the axial velocity profile using constraints that include Q_u and Q_o, effectively making this velocity profile dependent on F_s. Additionally, the trajectory space was expanded to include the cylindrical hydrocyclone segment, the computational load was reduced from 1s to 10ms, and the introduction of oil droplets were assumed uniformly distributed in inlet volume as opposed to inlet area.

Valve models with internal position control are ubiquitous in various process industries. As a result, there are several valve models to choose from for predicting actual valve opening from the commanded valve opening. A dynamic pin-cart model was proposed in Paper D to emulate the control valve from electrical valve input to actual valve opening percentage. The purpose of the pin-cart model was to describe a non-linear delay when changing direction. An experiment that continuously actuates the valve was used to test the performance of commonly used valve models, such as FOPDT and stiction, where the pin-cart model had the least estimation error, but also had the most model parameters.

Experimental validations and the challenges associated with using an OiW dispersion were addressed in Paper E. Measurements of OiW concentrations were obtained from fluorescence-based OiW monitors that were installed on the hydrocyclone inlet and underflow sidestreams as part of the modified pilot plant. To improve the quality of the OiW measurements, two OiW monitors were installed on each sidestream. Additionally, the sidestream valves were carefully controlled to maintain a constant sidestream flow rate.

In conclusion, this thesis has combined various control-oriented modeling methodologies in the pursuit to describe the deoiling performance of a deoiling hydrocyclone. The knowledge of separation performance provided by the model enables higher-level control strategies to be deployed and defined based on a desired economic strategy, rather than controlling for intermediate variables, such as PDR and H_{water}. Besides control purposes, the proposed model may be utilized for its observer-based benefits, as a means to estimate the current performance to provide reasoning within the topic of FDD. The potential to lower the environmental footprint and/or reduce the operational costs can be achieved by plant-wide PWT control if the model proves to be accurate when implemented into offshore PWT systems.

7.2 Future Work

It is apparent that advanced models with several intermediate variables can nearly always benefit from additional validation. This is also the case for the intermediate variables of the proposed grey-box model. As OiW monitors are rising in popularity, it is valuable to follow the technological development of OiW monitors, for measuring droplet sizes and OiW concentration. The ODT model can be expanded to include effects such as droplet coalescence and breakup.

To reduce the gap between research and industrial implementation, the proposed model can be developed into an industrial-grade software tool. The model can be used in MPC solutions, with the purpose of minimizing cost while complying with discharge regulations. This involves defining an operational economic cost function and incorporating it in the MPC. Several operational and economic strategies can be proposed, so that operators may choose the most compelling strategy, or modify existing ones.

References

[1] EIA, "International Energy Outlook 2019: World Energy Projection System Plus," Washington, DC, 2019. [Online]. Available: www.eia.gov/aeo (Accessed 2020-07-07).

[2] M. T. Stephenson, "A Survey of Produced Water Studies," in *Produced Water*, ser. Environmental Science Research, J. P. Ray and F. R. Engelhardt, Eds. Boston, MA, USA: Springer, 1992, pp. 1–11. ISBN 978-1-4615-2902-6. doi: 10.1007/978-1-4615-2902-6_1

[3] J. A. Veil, M. G. Puder, D. Elcock, and J. Redweik, R. J., "A white paper describing produced water from production of crude oil, natural gas, and coal bed methane." Argonne National Laboratory, Argonne, IL, USA, Tech. Rep. 63, 2004. doi: 10.2172/821666

[4] B. Bailey, M. Crabtree, J. Tyrie, J. Elphick, F. Kuchuk, C. Romano, and L. Roodhart, "Water Control," in *Oilfield Review*, R. C. Hertzog and G. M. Gillis, Eds. Houston, TX, USA: Schlumberger, 2000, vol. 12, no. 1, pp. 30–51.

[5] J. C. Robinson, "Afternoon Wrap-Up: An overview of produced water treatment technologies," in *14th Annual International Petroleum Environmental Conference*, Houston, TX, USA, 2007.

[6] P. Janssen and C. Harris, "Emulsion Characteristics of High Water-cut Oil Wells," in *SPE Annual Technical Conference and Exhibition*. New Orleans, LA, USA: Society of Petroleum Engineers, 1998, pp. 405–414. doi: 10.2118/49077-MS

[7] M. Choi, "Hydrocyclone Produced Water Treatment for Offshore Developments," in *SPE Annual Technical Conference and Exhibition*. New Orleans, LA, USA: Society of Petroleum Engineers, 1990, pp. 473–480. doi: 10.2118/20662-MS

[8] Danish Energy Agency, "Resource Assessment and Production Forecasts," Danish Energy Agency, Copenhagen, Denmark, Tech. Rep., 2018.

[9] U. Ahmed, "Making The Most of Maturing Fields," in *Oilfield Review*, D. Williamson and R. Gir, Eds. Houston, TX, USA: Schlumberger, 2004, vol. 16, pp. 1–1.

[10] Danish Energy Agency, "Monthly and Yearly Production," 2018. [Online]. Available: https://ens.dk/en/our-services/oil-and-gas-related-data/monthly-and-yearly-production (Accessed 2020-02-18).

[11] F. Brette, B. Machado, C. Cros, J. P. Incardona, N. L. Scholz, and B. A. Block, "Crude Oil Impairs Cardiac Excitation-Contraction Coupling in Fish," *Science*, vol. 343, no. 6172, pp. 772–776, 2014. doi: 10.1126/science.1242747

[12] P. Ekins, R. Vanner, and J. Firebrace, "Zero emissions of oil in water from offshore oil and gas installations: economic and environmental implications," *Journal of Cleaner Production*, vol. 15, no. 13-14, pp. 1302–1315, 2007. doi: 10.1016/j.jclepro.2006.07.014

[13] T. Bakke, J. Klungsøyr, and S. Sanni, "Environmental impacts of produced water and drilling waste discharges from the Norwegian offshore petroleum industry," *Marine Environmental Research*, vol. 92, pp. 154–169, 2013. doi: 10.1016/j.marenvres.2013.09.012

[14] L. Hasselberg, S. Meier, and A. Svardal, "Effects of alkylphenols on redox status in first spawning Atlantic cod (Gadus morhua)," *Aquatic Toxicology*, vol. 69, no. 1, pp. 95–105, 2004. doi: 10.1016/j.aquatox.2004.04.004

[15] K. Hylland, "Polycyclic Aromatic Hydrocarbon (PAH) Ecotoxicology in Marine Ecosystems," *Journal of Toxicology and Environmental Health, Part A*, vol. 69, no. 1-2, pp. 109–123, 2007. doi: 10.1080/15287390500259327

[16] K. V. Thomas, K. Langford, K. Petersen, A. J. Smith, and K. E. Tollefsen, "Effect-Directed Identification of Naphthenic Acids As Important in Vitro Xeno-Estrogens and Anti-Androgens in North Sea Offshore Produced Water Discharges," *Environmental Science & Technology*, vol. 43, no. 21, pp. 8066–8071, 2009. doi: 10.1021/es9014212

[17] M. Yang, "Measurement of Oil in Produced Water," in *Produced Water*, 1st ed., K. Lee and J. M. Neff, Eds. New York, NY, USA: Springer, 2011, ch. 2, pp. 57–88. ISBN 978-1-4614-0045-5. doi: 10.1007/978-1-4614-0046-2_2

[18] R. Toril Inga, E. Garpestad, M. Tangvald, and T. Frost, "Results and Commitments from the Zero Discharge Work on Produced Water Discharges on the Norwegian Continental Shelf," in *Proceedings of SPE International Conference on Health, Safety, and Environment in Oil and Gas Exploration and Production*. Calgary, AB, Canada: Society of Petroleum Engineers, 2004, pp. 1327–1332. doi: 10.2523/86801-MS

[19] OSPAR Commission, "North Sea Manual on Maritime Oil Pollution Offences," OSPAR Commission, London, UK, Tech. Rep., 2010.

[20] Danish Environmental Protection Agency, "Generel tilladelse for Mærsk Olie og Gas A/S (Mærsk Olie) til anvendelse, udledning og anden bortskaffelse af stoffer og materialer, herunder olie og kemikalier i produktions- og injektionsvand fra produktionsenhederne Halfdan, Dan, Tyra og Gorm for perioden 1. januar 2017 - 31. december 2018," Danish Environmental Protection Agency, Copenhagen, Denmark, Tech. Rep., 2016.

[21] W. Georgie, "Effective and Holistic Approach to produced Water Management for Offshore Operation," in *Offshore Technology Conference*. Houston, TX, USA: Offshore Technology Conference, 2002, pp. 1–13. doi: 10.4043/14286-MS

[22] TÜV SÜD NEL, "An Introduction to Produced Water Management," TÜV SÜD NEL, Glasgow, UK, Tech. Rep., 2020.

[23] J. Coca-Prados, Gemma Gutiérrez-Cervelló, and J. M. Benito, "Treatment of Oily Wastewater," in *Water Purification and Management*, 1st ed., ser. NATO Science for Peace and Security Series C: Environmental Security, J. Coca-Prados and G. Gutiérrez-Cervelló, Eds. Dordrecht, Netherlands: Springer, 2011, ch. 1, pp. 1–55. ISBN 9789400750784. doi: 10.1007/978-90-481-9775-0_1

[24] M. F. Schubert, F. Skilbeck, and H. J. Walker, "Liquid Hydrocyclone Separation Systems," in *Hydrocyclones*, 1st ed., ser. Fluid Mechanics and Its Applications, L. Svarovsky and M. Thew, Eds. Dordrecht, Netherlands: Springer, 1992, vol. 12, pp. 275–293. ISBN 978-90-481-4180-7. doi: 10.1007/978-94-015-7981-0_18

[25] K. Arnold and M. Stewart, *Surface Production Operations: Design of Oil-Handling Systems and Facilities*, 2nd ed. Elsevier, 1999, vol. 1. ISBN 9780884158219. doi: 10.1016/B978-0-88415-821-9.X5000-3

[26] T. Husveg, O. Rambeau, T. Drengstig, and T. Bilstad, "Performance of a deoiling hydrocyclone during variable flow rates," *Minerals Engineering*, vol. 20, no. 4, pp. 368–379, 2007. doi: 10.1016/j.mineng.2006.12.002

[27] A. Fakhru'l-Razi, A. Pendashteh, L. C. Abdullah, D. R. A. Biak, S. S. Madaeni, Z. Z. Abidin, A. Fakhru'l-Razi, A. Pendashteh, L. C. Abdullah, D. R. A. Biak, S. S. Madaeni, and Z. Z. Abidin, "Review of technologies for oil and gas produced water treatment," *Journal of Hazardous Materials*, vol. 170, no. 2-3, pp. 530–551, 2009. doi: 10.1016/j.jhazmat.2009.05.044

[28] Alderley, "Produced Water Treatment," Wickwar, UK, Tech. Rep., 2003.

[29] A. F. Sayda and J. H. Taylor, "Modeling and Control of Three-Phase Gravilty Separators in Oil Production Facilities," in *2007 American Control Conference*. New York, NY, USA: IEEE, 2007, pp. 4847–4853. doi: 10.1109/ACC.2007.4282265

[30] G. Young, W. Wakley, D. Taggart, S. Andrews, and J. Worrell, "Oil-water separation using hydrocyclones: An experimental search for optimum dimensions," *Journal of Petroleum Science and Engineering*, vol. 11, no. 1, pp. 37–50, 1994. doi: 10.1016/0920-4105(94)90061-2

[31] K. L. Jepsen, "Modeling and Control of Membrane Filtration Systems for Offshore Produced Water Treatment," Ph.D. Thesis, Aalborg University, Aalborg, Denmark. ISBN 978-87-7210-409-6 2019.

[32] D. F. Kelsall, "A Study of the Motion of Solid Particles in a Hydraulic Cyclone," *Chemical Engineering Research and Design*, vol. 30, pp. 87–108, 1952.

[33] K. Rietema, "Performance and design of hydrocyclones—I: General considerations," *Chemical Engineering Science*, vol. 15, no. 3-4, pp. 298–302, 1961. doi: 10.1016/0009-2509(61)85033-1

[34] M. Thew, "Cyclones for Oil/Water Separations," in *Encyclopedia of Separation Science*, I. D. Wilson, Ed. Oxford: Academic Press, 2000, pp. 1480–1490. ISBN 978-0-12-226770-3. doi: 10.1016/B0-12-226770-2/04601-9

[35] S. Amini, D. Mowla, and M. Golkar, "Developing a new approach for evaluating a de-oiling hydrocyclone efficiency," *Desalination*, vol. 285, pp. 131–137, 2012. doi: 10.1016/j.desal.2011.09.044

[36] J. Tian, L. Ni, T. Song, J. Olson, and J. Zhao, "An overview of operating parameters and conditions in hydrocyclones for enhanced separations," *Separation and Purification Technology*, vol. 206, pp. 268–285, 2018. doi: 10.1016/j.seppur.2018.06.015

[37] D. Colman and M. Thew, "Correlation of separation results from light dispersion hydrocyclones," *Chemical Engineering Research and Design*, vol. 61, no. 4, pp. 233–240, 1983.

[38] P. Jones, "A Field Comparison of Static and Dynamic Hydrocyclones," *SPE Production & Facilities*, vol. 8, no. 2, pp. 84–90, 1993. doi: 10.2118/20701-PA

[39] A. Sinker, M. Humphris, and N. Wayth, "Enhanced Deoiling Hydrocyclone Performance without Resorting to Chemicals," in *SPE Offshore Europe Oil and Gas Conference and Exhibition*. Aberdeen, UK: Society of Petroleum Engineers, 1999, pp. 1–9. doi: 10.2118/56969-MS

[40] P. Durdevic and Z. Yang, "Application of H_∞ Robust Control on a Scaled Offshore Oil and Gas De-oiling Facility," *Energies*, vol. 11, no. 2, pp. 1–18, 2018. doi: 10.3390/en11020287

[41] A. Sausen, P. Sausen, and M. de Campos, "The Slug Flow Problem in Oil Industry and Pi Level Control," in *New Technologies in the Oil and Gas Industry*, J. S. Gomes, Ed. InTech Open Access Publisher, 2012, ch. 5, pp. 103–118. doi: 10.5772/50711

[42] N. Meldrum, "Hydrocyclones: A Solutlon to Produced-Water Treatment," *SPE Production Engineering*, vol. 3, no. 4, pp. 669–676, 1988. doi: 10.2118/16642-PA

[43] A. Belaidi and M. T. Thew, "The effect of oil and gas content on the controllability and separation in a De-oiling hydrocyclone," *Chemical Engineering Research and Design*, vol. 81, no. 3, pp. 305–314, 2003. doi: 10.1205/02638760360596856

[44] M. T. Thew and I. C. Smyth, "Development and performance of oil-water hydrocyclone separators: A review," in *Proceedings of IMM Conference on Innovation in Physical Separation Technologies*. London, UK: Institute of Materials, Minerals and Mining, 1998, pp. 77–89.

[45] L. R. Plitt, "A Mathematical Model of The Hydrocyclone Classifier," *CIM Bulletin*, vol. 69, no. 776, pp. 114–123, 1976.

[46] L. Svarovsky and J. Svarovsky, "A New Method of Testing Hydrocyclone Grade Efficiencies," in *Hydrocyclones*, 1st ed., ser. Fluid Mechanics and Its Applications, M. Thew and L. Svarovsky, Eds. Dordrecht, Netherlands: Springer, 1992, vol. 12, pp. 135–145. ISBN 978-90-481-4180-7. doi: 10.1007/978-94-015-7981-0_10

[47] N. Kharoua, L. Khezzar, and Z. Nemouchi, "Hydrocyclones for De-oiling Applications—A Review," *Petroleum Science and Technology*, vol. 28, no. 7, pp. 738–755, 2010. doi: 10.1080/10916460902804721

[48] P. Durdevic, S. Pedersen, and Z. Yang, "Challenges in Modelling and Control of Offshore De-oiling Hydrocyclone Systems," *Journal of Physics: Conference Series*, vol. 783, pp. 1–10, 2017. doi: 10.1088/1742-6596/783/1/012048

[49] P. Durdevic, S. Pedersen, and Z. Yang, "Operational performance of offshore de-oiling hydrocyclone systems," in *IECON 2017 - 43rd Annual Conference of the IEEE Industrial Electronics Society*. Beijing, China: IEEE, 2017, pp. 6905–6910. doi: 10.1109/IECON.2017.8217207

[50] Zhenyu Yang, S. Pedersen, and P. Durdevic, "Cleaning the produced water in offshore oil production by using plant-wide optimal control strategy," in *2014 Oceans St. John's*. St. John's, NL, Canada: IEEE, 2014, pp. 1–10. doi: 10.1109/OCEANS.2014.7003038

[51] T. Das and J. Jäschke, "Modeling and control of an inline deoiling hydrocyclone," *IFAC-PapersOnLine*, vol. 51, no. 8, pp. 138–143, 2018. doi: 10.1016/j.ifacol.2018.06.368

[52] T. Das, S. J. Heggheim, M. Dudek, A. Verheyleweghen, and J. Jäschke, "Optimal Operation of a Subsea Separation System Including a Coalescence Based Gravity Separator Model and a Produced Water Treatment Section," *Industrial and Engineering Chemistry Research*, vol. 58, no. 10, pp. 4168–4185, 2019. doi: 10.1021/acs.iecr.8b04923

[53] Z. Yang, J. P. Stigkær, and B. Løhndorf, "Plant-wide Control for Better De-oiling of Produced Water in Offshore Oil & Gas Production," *IFAC Proceedings Volumes*, vol. 46, no. 20, pp. 45–50, 2013. doi: 10.3182/20130902-3-CN-3020.00143

[54] M. V. Bram, A. A. Hassan, D. S. Hansen, P. Durdevic, S. Pedersen, and Z. Yang, "Experimental modeling of a deoiling hydrocyclone system," in *20th International Conference on Methods and Models in Automation and Robotics, MMAR*, no. 1. Miedzyzdroje, Poland: IEEE, 2015, pp. 1080–1085. doi: 10.1109/MMAR.2015.7284029

[55] P. Durdevic, S. Pedersen, M. V. Bram, D. Hansen, A. Hassan, and Z. Yang, "Control Oriented Modeling of a De-oiling Hydrocyclone," *IFAC-PapersOnLine*, vol. 48, no. 28, pp. 291–296, 2015. doi: 10.1016/j.ifacol.2015.12.141

[56] P. Durdevic and Z. Yang, "Dynamic Efficiency Analysis of an Off-Shore Hydrocyclone System, Subjected to a Conventional PID- and Robust-Control-Solution," *Energies*, vol. 11, no. 9, pp. 1–14, 2018. doi: 10.3390/en11092379

[57] S. J. Ohrem, H. Kim, M. A. Lundteigen, and C. Holden, "A Comparison of Hazards and Efficiencies of Conventional and Adaptive Control Algorithms Using Systems-Theoretic Process Analysis," *MATEC Web of Conferences*, vol. 273, pp. 1–19, 2019. doi: 10.1051/matecconf/201927302006

[58] L. Hansen, P. Durdevic, K. L. Jepsen, and Z. Yang, "Plant-wide Optimal Control of an Offshore De-oiling Process Using MPC Technique," *IFAC-PapersOnLine*, vol. 51, no. 8, pp. 144–150, 2018. doi: 10.1016/j.ifacol.2018.06.369

[59] L. Ma, P. Fu, J. Wu, F. Wang, J. Li, Q. Shen, and H. Wang, "CFD Simulation Study on Particle Arrangements at the Entrance to a Swirling Flow Field for Improving the Separation Efficiency of Cyclones," *Aerosol and Air Quality Research*, vol. 15, no. 6, pp. 2456–2465, 2015. doi: 10.4209/aaqr.2015.02.0126

[60] Y. R. Murthy and K. U. Bhaskar, "Parametric CFD studies on hydrocyclone," *Powder Technology*, vol. 230, pp. 36–47, 2012. doi: 10.1016/j.powtec.2012.06.048

[61] M. F. Dlamini, M. S. Powell, and C. J. Meyer, "A CFD simulation of a single phase hydrocyclone flow field," *Journal of the South African Institute of Mining and Metallurgy*, vol. 105, no. 10, pp. 711–717, 2005.

[62] A. Motin, "Theoretical and numerical study of swirling flow separation devices for oil-water mixtures," Ph.D. Thesis, Michigan State University, Lansing, MI, USA. ISBN 9781339256214 2015.

[63] K. U. Bhaskar, Y. R. Murthy, M. R. Raju, S. Tiwari, J. Srivastava, and N. Ramakrishnan, "CFD simulation and experimental validation studies on hydrocyclone," *Minerals Engineering*, vol. 20, no. 1, pp. 60–71, 2007. doi: 10.1016/j.mineng.2006.04.012

[64] H. Eren, C. Fung, K. Wong, and A. Gupta, "Artificial neural networks in estimation of hydrocyclone parameter d50c with unusual input variables," *IEEE Transactions on Instrumentation and Measurement*, vol. 46, no. 4, pp. 908–912, 1997. doi: 10.1109/19.650798

[65] K. W. Wong, Y. S. Ong, H. Eren, and C. C. Fung, "Hybrid fuzzy modelling using memetic algorithm for hydrocyclone control," in *Proceedings of 2004 International Conference on Machine Learning and Cybernetics (IEEE Cat. No.04EX826)*, vol. 7. Shanghai, China: IEEE, 2004, pp. 4188–4193. doi: 10.1109/icmlc.2004.1384574

[66] S. J. Ohrem, T. T. Kristoffersen, and C. Holden, "Model-Based and Model-Free Optimal Control of a Gas Liquid Cylindrical Cyclone," *IFAC-PapersOnLine*, vol. 51, no. 8, pp. 113–119, 2018. doi: 10.1016/j.ifacol.2018.06.364

[67] J. Peel, C. Howarth, and C. Ramshaw, "Process Intensification: Higee Seawater Deaeration," *Chemical Engineering Research and Design*, vol. 76, no. 5, pp. 585–593, 1998. doi: 10.1205/026387698525261

[68] K. Rietema, "The mechanism of the separation of finely dispersed solids in cyclones," in *Cyclones in industry*, K. Rietema and C. Verver, Eds. Amsterdam, Netherlands: Elsevier, 1961, pp. 46–63.

[69] B. F. Ma, "Purification of Waste Waters from Petroleum Industry by Hydrocyclone. Development of a New Three-Phase Hydrocyclone," Ph.D. Thesis, INSA Toulouse, Toulouse, France, 1993.

[70] D. Wolbert, B. F. Ma, Y. Aurelle, and J. Seureau, "Efficiency estimation of liquid-liquid Hydrocyclones using trajectory analysis," *AIChE Journal*, vol. 41, no. 6, pp. 1395–1402, 1995. doi: 10.1002/aic.690410606

[71] T. Husveg, O. Johansen, and T. Bilstad, "Operational Control of Hydrocyclones During Variable Produced Water Flow Rates - Frøy Case Study," *SPE Production & Operations*, vol. 22, no. 3, pp. 294–300, 2007. doi: 10.2118/100666-PA

[72] M. Shoukat Choudhury, N. Thornhill, and S. Shah, "Modelling valve stiction," *Control Engineering Practice*, vol. 13, no. 5, pp. 641–658, 2005. doi: 10.1016/j.conengprac.2004.05.005

[73] R. Bacci di Capaci and C. Scali, "Review and comparison of techniques of analysis of valve stiction: From modeling to smart diagnosis," *Chemical Engineering Research and Design*, vol. 130, pp. 230–265, 2018. doi: 10.1016/j.cherd.2017.12.038

[74] J. J. Derksen and H. E. A. Van den Akker, "Simulation of vortex core precession in a reverse-flow cyclone," *AIChE Journal*, vol. 46, no. 7, pp. 1317–1331, 2000. doi: 10.1002/aic.690460706

[75] D. Colman, "The Hydrocyclone for Separating Light Dispersions," Ph.D. Thesis, University of Southampton, Southampton, UK, 1981.

[76] B. Dabir and C. A. Petty, "Measurements of mean velocity profiles in a hydrocyclone using laser doppler anemometry," *Chemical Engineering Communications*, vol. 48, no. 4-6, pp. 377–388, 1986. doi: 10.1080/00986448608910025

[77] Luo Qian and J. R. Xu, "The Effect of the Air Core on the Flow Field within Hydrocyclones," in *Hydrocyclones*, 1st ed., ser. Fluid Mechanics and Its Applications, L. Svarovsky and M. Thew, Eds. Dordrecht, Netherlands: Springer, 1992, vol. 12, pp. 51–62. ISBN 978-90-481-4180-7. doi: 10.1007/978-94-015-7981-0_4

[78] D. Colman and M. Thew, "Hydrocyclone to Give a Highly Concentrated Sample of a Lighter Dispersed Phase," in *1st International Conference on Hydrocyclones*, G. Priestley and H. Stephens, Eds. Cambridge, UK: BHRA Fluid Engineering, 1980, pp. 209–223.

[79] B. Zhao, "Development of a new method for evaluating cyclone efficiency," *Chemical Engineering and Processing: Process Intensification*, vol. 44, no. 4, pp. 447–451, 2005. doi: 10.1016/j.cep.2004.06.007

[80] S. Amini, D. Mowla, M. Golkar, and F. Esmaeilzadeh, "Mathematical modelling of a hydrocyclone for the down-hole oil-water separation (DOWS)," *Chemical Engineering Research and Design*, vol. 90, no. 12, pp. 2186–2195, 2012. doi: 10.1016/j.cherd.2012.05.007

[81] D. S. Hansen, S. Jespersen, M. V. Bram, and Z. Yang, "Uncertainty Analysis of Fluorescence-Based Oil-In-Water Monitors for Oil and Gas Produced Water," *Sensors*, vol. 20, no. 16, pp. 1–36, 2020. doi: 10.3390/s20164435

[82] E. Blanchard, "Oil in water monitoring is a key to production separation," *Offshore*, vol. 73, no. 11, pp. 104–105, 2013.

[83] M. Vallabhan and C. Holden, "Non-linear control algorithms for de-oiling hydrocyclones," in *2020 28th Mediterranean Conference on Control and Automation (MED)*, no. 978. Saint-Raphaël, France: IEEE, 2020, pp. 85–90. doi: 10.1109/MED48518.2020.9183115

[84] D. S. Hansen, M. V. Bram, and Z. Yang, "Efficiency investigation of an offshore deoiling hydrocyclone using real-time fluorescence- and microscopy-based monitors," in *2017 IEEE Conference on Control Technology and Applications (CCTA)*. Mauna Lani, HI, USA: IEEE, 2017, pp. 1104–1109. doi: 10.1109/CCTA.2017.8062606

[85] P. Durdevic, C. S. Raju, M. V. Bram, D. S. Hansen, and Z. Yang, "Dynamic oil-in-water concentration acquisition on a pilot-scaled offshore water-oil separation facility," *Sensors*, vol. 17, no. 1, pp. 1–11, 2017. doi: 10.3390/s17010124

[86] P. Durdevic, S. Pedersen, and Z. Yang, "Evaluation of OiW measurement technologies for deoiling hydrocyclone efficiency estimation and control," in *OCEANS 2016 - Shanghai*. Shanghai, China: IEEE, 2016, pp. 1–7. doi: 10.1109/OCEANSAP.2016.7485361

[87] M. V. Bram, L. Hansen, D. S. Hansen, and Z. Yang, "Grey-Box modeling of an offshore deoiling hydrocyclone system," in *2017 IEEE Conference on Control Technology and Applications (CCTA)*. Mauna Lani, HI, USA: IEEE, 2017, pp. 94–98. doi: 10.1109/CCTA.2017.8062446

[88] M. V. Bram, L. Hansen, D. S. Hansen, and Z. Yang, "Hydrocyclone Separation Efficiency Modeled by Flow Resistances and Droplet Trajectories," *IFAC-PapersOnLine*, vol. 51, no. 8, pp. 132–137, 2018. doi: 10.1016/j.ifacol.2018.06.367

[89] M. V. Bram, L. Hansen, D. S. Hansen, and Z. Yang, "Extended Grey-Box Modeling of Real-Time Hydrocyclone Separation Efficiency," in *2019 18th European Control Conference (ECC)*. Naples, Italy: IEEE, 2019, pp. 3625–3631. doi: 10.23919/ECC.2019.8796175

[90] M. V. Bram, J. P. Calliess, S. Roberts, D. S. Hansen, and Z. Yang, "Analysis and Modeling of State-Dependent Delay in Control Valves," *IFAC-PapersOnLine*, 2020, [Accepted/In press].

[91] M. V. Bram, S. Jespersen, D. S. Hansen, and Z. Yang, "Control-Oriented Modeling and Experimental Validation of a Deoiling Hydrocyclone System," *Processes*, vol. 8, no. 9, pp. 1–33, 2020. doi: 10.3390/pr8091010

[92] K. Rajamani and K. Hsieh, "Hydrocyclone model: A fluid mechanic approach," in *SME Annual Meeting*, S. G. D. Smith, Ed. Phoenix, AZ, USA: Society of Mining Engineers of AIME, 1988, pp. 1–8.

[93] W. Wei, J. Y. Yu, X. T. Zheng, L. Xia, and L. Wei, "A New Method for Predicting the Hydrocyclone Efficiency with the Light Dispersed Phase," *Energy Procedia*, vol. 105, pp. 4428–4435, 2017. doi: 10.1016/j.egypro.2017.03.939

[94] D. J. Spottiswood and E. Kelly, *Introduction to Mineral Processing*. New York, NY, USA: John Wiley & Sons, 1982. ISBN 0471033790

[95] A. Motin, V. V. Tarabara, C. A. Petty, and A. Bénard, "Hydrodynamics within flooded hydrocyclones during excursion in the feed rate: Understanding of turndown ratio," *Separation and Purification Technology*, vol. 185, pp. 41–53, 2017. doi: 10.1016/j.seppur.2017.05.015

[96] R. K. Rajamani and L. Milin, "Fluid-flow model of the hydrocyclone for concentrated slurry classification," in *Hydrocyclones*, 1st ed., ser. Fluid Mechanics and Its Applications, L. Svarovsky and M. Thew, Eds. Dordrecht, Netherlands: Springer, 1992, vol. 12, pp. 95–108. ISBN 978-90-481-4180-7. doi: 10.1007/978-94-015-7981-0_7

[97] E. Ortega-Rivas and L. Svarovsky, "Effect of solids feed grade on the separation of slurries in hydrocyclones," in *Hydrocyclones*, 1st ed., ser. Fluid Mechanics and Its Applications, L. Svarovsky and M. Thew, Eds. Dordrecht, Netherlands: Springer, 1992, vol. 12, pp. 147–175. ISBN 978-90-481-4180-7. doi: 10.1007/978-94-015-7981-0_11

[98] R. R. Horsley, Q.-K. Tran, and J. A. Reizes, "The effect of rheology on the performance of hydrocyclones," in *Hydrocyclones*, 1st ed., ser. Fluid Mechanics and Its Applications, L. Svarovsky and M. Thew, Eds. Dordrecht, Netherlands: Springer, 1992, vol. 12, pp. 215–227. ISBN 978-90-481-4180-7. doi: 10.1007/978-94-015-7981-0_14

[99] K. T. Hsieh and R. K. Rajamani, "Mathematical model of the hydrocyclone based on physics of fluid flow," *AIChE Journal*, vol. 37, no. 5, pp. 735–746, 1991. doi: 10.1002/aic.690370511

[100] L. Desborough and R. Miller, "Increasing customer value of industrial control performance monitoring - Honeywell's experience," *AIChE symposium series*, vol. 98, no. 326, pp. 169–189, 2002.

[101] M. Choudhury, N. Thornhill, and S. Shah, "A Data-Driven Model for Valve Stiction," *IFAC Proceedings Volumes*, vol. 37, no. 1, pp. 245–250, 2004. doi: 10.1016/S1474-6670(17)38739-6

[102] M. A. Choudhury, V. Kariwala, S. L. Shah, H. Douke, H. Takada, and N. F. Thornhill, "A simple test to confirm control valve stiction," *IFAC Proceedings Volumes*, vol. 16, no. 1, pp. 81–86, 2005. doi: 10.3182/20050703-6-CZ-1902.01589

[103] M. Jelali, "An overview of control performance assessment technology and industrial applications," *Control Engineering Practice*, vol. 14, no. 5, pp. 441–466, 2006. doi: 10.1016/j.conengprac.2005.11.005

[104] S. Pedersen, "Plant-Wide Anti-Slug Control for Offshore Oil and Gas Processes," Ph.D. Thesis, Aalborg University, Aalborg, Denmark. ISBN 978-87-7112-796-6 2016. doi: 10.5278/vbn.phd.engsci.00183

[105] P. Durdevic, "Real-Time Monitoring and Robust Control of Offshore De-oiling Processes," Ph.D. Thesis, Aalborg University, Aalborg, Denmark. ISBN 978-87-7112-930-4 2017.

Part II

Papers

Paper A

Grey-Box Modeling of an Offshore Deoiling Hydrocyclone System

Mads V. Bram, Leif Hansen, Dennis S. Hansen, and Zhenyu Yang.

The paper has been published in
Proceedings of IEEE Conference on Control Technology and Applications (CCTA),
Mauna Lani, HI, pp. 806-811, 2017

The layout has been revised.

Paper B

Hydrocyclone Separation Efficiency Modeled by Flow Resistances and Droplet Trajectories

Mads V. Bram, Leif Hansen, Dennis S. Hansen, and Zhenyu Yang.

The paper has been published in
Proceedings of the IFAC workshop on Automatic Control in Offshore Oil and Gas Production (OOGP), Esbjerg, Denmark, Vol. 51, No. 8, pp. 132-137, 2018

The layout has been revised.

Paper C

Extended Grey-Box Modeling of Real-Time Hydrocyclone Separation Efficiency

Mads V. Bram, Leif Hansen, Dennis S. Hansen, and Zhenyu Yang.

The paper has been submitted to
Proceedings of the European Control Conference (ECC), Naples, Italy, pp. 3625-3631, 2018

The layout has been revised.

Paper D

Analysis and Modeling of State-Dependent Delay in Control Valves

Mads V. Bram, Jan-Peter Calliess, Stephen Roberts, Dennis S. Hansen, and Zhenyu Yang.

The paper has been published in
Proceedings of the IFAC World Congress, Germany, 2020

The layout has been revised.

Paper E

Control-Oriented Modeling and Experimental Validation of a Deoiling Hydrocyclone System

Mads V. Bram, Stefan Jespersen, Dennis S. Hansen, and Zhenyu Yang.

The paper has been published in
Processes (MDPI) Vol. 8(9), pp. 1-33, 2020.

The layout has been revised.

ISSN (online): 2446-1636
ISBN (online): 978-87-7210-814-8 AALBORG UNIVERSITY PRESS